



# Coherent State Wave Functions on the Torus

Mikael Fremling

Licentiate Thesis

Akademisk avhandling  
för avläggande av licentiatexamen i teoretisk fysik  
vid Stockholms Universitet

Department of Physics  
Stockholm University

Maj 2013



## Abstract

In the study of the quantum Hall effect there are still many unresolved problems. One of these is how to generate representative wave functions for ground states on other geometries than the planar and spherical. We study one such geometry, the toroidal one, where the periodic boundary conditions must be properly taken into account.

As a tool to study the torus we investigate the properties of various types of localized states, similar to the *coherent states* of the harmonic oscillator, which are maximally localized in phase space. We consider two alternative definitions of localized states in the lowest Landau level (LLL) on a torus. One is the projection of the coordinate delta function onto the LLL. Another definition, proposed by Haldane & Rezayi, is to consider the set of functions which have all their zeros at a single point. Since all LLL wave functions on a torus, are uniquely defined by the position of their zeros, this defines a set of functions that are expected to be localized around the point maximally far away from the zeros.

These two families of localized states have many properties in common with the coherent states on the plane and on the sphere, *e.g.* a simple resolution of unity and a simple self-reproducing kernel. However, we show that only the projected delta function is maximally localized.

We find that because of modular covariance, there are severe restrictions on which wave functions that are acceptable on the torus. As a result, we can write down a trial wave function for the  $\nu = \frac{2}{5}$  state, that respects the modular covariance, and has good numerical overlap with the exact coulomb ground state.

Finally we present preliminary calculations of the antisymmetric component of the viscosity tensor for the proposed, modular covariant,  $\nu = \frac{2}{5}$  state, and find that it is in agreement with theoretical predictions.

## Acknowledgements

I would like to thank my two supervisors Hans Hansson and Anders Karlhede for support and inspiration. It must be frustrating when minor bugs change the result from success to failure and back again. Thank you all friends and colleagues who in one way or another have contributed to this thesis, whether it be proofreading, being bugged with questions or just general discussions. A special thanks goes to Gertrud Fremling for thoroughly proofreading the manuscript, I do not want to think of what it would have looked like if you had not. I would also like to thank my wife, Karin Fremling, who has not only put up with my frequent absentmindedness, but also encouraged my work wholeheartedly.

Finally, I would like to thank YOU, the reader of this thesis, for showing an interest in my work.

Thank you!

# Contents

<b>List of Acompaining Papers</b>	<b>5</b>
<b>1 Introduction and Outline</b>	<b>6</b>
<b>2 The Quantum Hall Effect</b>	<b>8</b>
2.1 The Classical Hall Effect . . . . .	8
2.2 The Quantum Hall Effect . . . . .	8
2.3 The Laughlin Construction and the Hierarchy . . . . .	11
2.4 Composite Fermions . . . . .	11
2.5 Fractional Quantum Hall Effect on a Torus . . . . .	12
<b>3 Coherent States in a Magnetic Field</b>	<b>13</b>
3.1 Coherent States in the Harmonic Oscillator . . . . .	13
3.2 Coherent States in a Magnetic Field in Planar Geometry . . . . .	14
3.3 The Torus Itself . . . . .	17
3.4 Basis states . . . . .	18
3.5 Lattice Coherent States (LCS) . . . . .	19
3.6 Continuous Coherent states (CCS) . . . . .	22
3.7 Localization behaviour of LCS and CCS . . . . .	25
3.7.1 The low flux limit $N_s = 1, 2, 3, 4$ . . . . .	25
3.7.2 The Thermodynamic limit $N_s \rightarrow \infty$ . . . . .	26
3.7.3 Changing the Aspect Ratio of the Torus . . . . .	26
3.7.4 Changing the Skewness of the Torus . . . . .	27
<b>4 Trial Wave Functions from CFT</b>	<b>30</b>
4.1 A Concrete Example: The Modified Laughlin State . . . . .	32
4.2 Numerical evaluation of $\psi^{(q,p)}$ . . . . .	35
4.2.1 How to Treat the Derivatives in Many-Particle States . . . . .	36
4.2.2 The Requirement of Modular Covariance . . . . .	39
<b>5 Viscosity in FQHS</b>	<b>42</b>
5.1 Viscosity in the $\nu = \frac{2}{5}$ State . . . . .	43
<b>6 Summary and Outlook</b>	<b>46</b>
<b>A Jacobi Theta Functions and some Relations</b>	<b>48</b>

# List of accompanying papers

- Paper I    **Coherent State Wave Functions on a  
Torus with a Constant Magnetic Field**  
M. Fremling  
J. Phys. A, under consideration [arXiv:1302.6471] (2013)
- Paper II   **Hall viscosity of hierarchical  
quantum hall states.**  
M. Fremling, T. H. Hansson, and J. Suorsa.  
In preparation, (2013)

# Chapter 1

## Introduction and Outline

This year marks the 30 year anniversary of Laughlin's famous  $\nu = \frac{1}{3}$  wave function, introduced to explain the Fractional Quantum Hall Effect. With the Laughlin wave function came the notion of excitations with fractional charge, and fractional statistics. The theory of the Quantum Hall Effect is still an active area of research. The Integer Hall Effect was the first example of a Topological Insulator[14], but many others have been proposed and realized. Fractional charges have also been proposed to exist in other types of systems, where fractional Chern Insulators are a case in point[24]. Vivid research has also been focused on the special state at  $\nu = \frac{5}{2}$ . This state is expected to support excitations with non-abelian braiding properties. The non-abelian statistics makes this state of matter an interesting candidate for quantum information storage and processing; in short, a quantum computer.

In quantum mechanics, the existence of a magnetic field drastically alters the structure of the Hilbert space as compared to the case of free particles. The continuum of energy levels of the free particle, transforms into highly degenerate Landau levels with a degeneracy proportional to the strength of the magnetic field. If the applied magnetic field is strong enough, together with low temperatures, and clean samples, the Quantum Hall Effect is observed. The Fractional Quantum Hall Effect (FQHE) is observed in high quality semiconductor junctions, but also in graphene. In semiconductors the temperature has to be low for the FQHE to be manifested, but in graphene the effect is observable even at room temperature[21].

Both the Integer and the Fractional Quantum Hall Effects are examples of Topological Insulators; States of matter that are insulating in the bulk, but has dissipationless transport at the edges. The topological aspect of the FQHE is that it is insensitive to continuous deformations of the geometry of a sample, but also to small variations of the applied magnetic field, or temperature. Most importantly, the dissipationless edge currents even survive a finite amount of impurities, which is always present in a real system. A consequence of this is that the electric resistance  $R_H$  is quantized, to an experimentally very high accuracy.

The topology of a state is important, and not all probes can detect topological quantities. Especially local measurement should not be able to distinguish between a topological and a trivial insulator.

In this thesis we are studying the FQHE on the torus. This is interesting as one of the topological aspect is encoded in the ground state degeneracy on the torus. The torus is also a good playground to test model trial functions coming from Conformal Field Theory (CFT). Trial wave functions for the FQHE have been deduced using correlators from CFT. The CFT wave functions are easily evaluated in a planar geometry, but numerical comparison to exact coulomb ground states can be difficult to perform because of boundary effects. The torus represents a natural arena to for numerical tests.

When constructing FQH-wave functions, the CFT trial wave functions need to be projected to the lowest Landau Level, to obtain physical electronic wave functions. The projector to the lowest Landau Level can naturally be expressed in terms of coherent states. For that reason a more careful study of coherent states on a toroidal geometry is needed. In this thesis we study the basic properties of coherent states on a torus. We consider study two kinds of coherent states, and their various properties.

In addition to studying coherent states on a torus we also investigate how to generate trial wave functions on the torus, in a self-consistent manner. As a result we find that modular properties strongly constrain the possible wave functions on the torus, and we propose a trial wave function for the  $\nu = \frac{2}{5}$  state that has the correct modular properties.

Using the proposed wave function, we calculate a topological characteristic of the quantum Hall system; the antisymmetric component of the viscosity tensor. Read has demonstrated that the viscosity is proportional to the mean orbital spin of the electron, which is a topological quantity. This transport coefficient can be measured numerically by changing the geometry of the torus[23].

This thesis has two accompanying papers. The first is my own work on coherent states, and the second, in preparation, is in collaboration with my supervisor Thors Hans Hansson, and Juha Suorsa at Nordita.



## Chapter 2

# The Quantum Hall Effect

### 2.1 The Classical Hall Effect

In 1879 the American physicist Edwin Hall decided to test whether or not electric currents were affected by magnetic forces[10]. He designed an experiment in which he found that a thin metal plate in a magnetic field  $\mathbf{B}$ , perpendicular to the surface of the plate, will experience a voltage drop in a direction perpendicular to  $\mathbf{B}$  and the current  $\mathbf{I}$  flowing through the plate. He concluded that the perpendicular resistance  $R_H = \frac{V}{I}$  was proportional to the strength of the magnetic field and sensitive to the sign of the magnetic field.

The Hall Effect is explained by the behaviour of charged particles in a magnetic field. As the electrons move through the magnetic field, they will be subject to a Lorentz force  $\mathbf{F}_B = q\mathbf{v} \times \mathbf{B}$  directed toward one of the edges of the plate. As more and more electrons are diverted toward one side, a charge imbalance built up inside the plate generating an electric field across the plate. The existence of a static electric field means that there is a voltage difference, which in this case will be perpendicular to the direction of the current  $\mathbf{I}$ . Eventually the electric field, with the associated electric force  $\mathbf{F}_E = q\mathbf{E}$ , will be large enough to balance the magnetic force  $\mathbf{F}_B$ . This voltage drop must be proportional to the total current, as a larger current increases the number of electrons that are being diverted. The voltage difference must also be proportional to the magnetic field, as the Lorentz force that deflects electrons is proportional in strength to  $B$ . Hence, the Hall resistance, which is the perpendicular resistance  $R_H$ , is proportional to the strength of magnetic field  $R_H \propto B$ . The Hall Effect is also inversely proportional to the thickness of the material the current runs through, which means that the Hall Effect gets stronger the thinner the plate is. A more careful analysis shows that the Hall Resistance is  $R_H = \frac{B}{e\rho_{3D}d}$ , where  $d$  is the thickness of the plate, and  $\rho_{3D}$  is the electron density. In the limit of very thin plates, that are almost two dimensional,  $R_H$  is better described using the two dimensional density  $\rho_{2D}$ , as  $R_H = \frac{B}{e\rho_{2D}}$ . It is in this limit of thin plates that quantum mechanical effects can become important, and the Hall Effect can be changed into the Quantum Hall Effect.

### 2.2 The Quantum Hall Effect

In 1980 von Klitzing gave the Hall Effect a new twist[15] by confining electrons to two dimensions, in semiconductor junctions. In his experiments, where he had high quality samples in combination with low temperatures and high magnetic fields, the Hall resistance  $R_H$  deviated from the classically predicted linear behaviour and instead started developing kinks and plateaus. Furthermore, these plateaus appeared at regular intervals such that the resistance at the

### The Hall Experiment

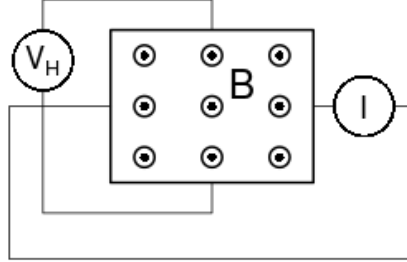
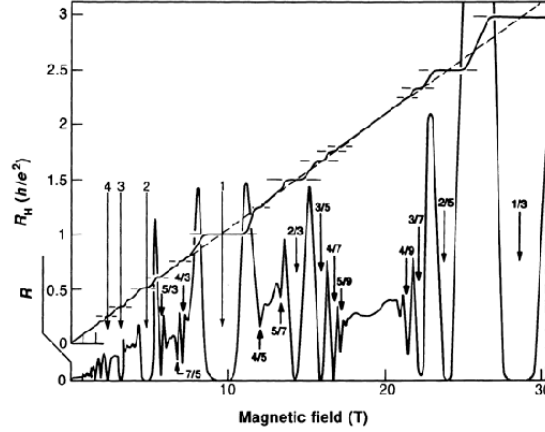


Figure 2.1: The Hall experiment. A current  $I$  is driven through a thin metal plate with a perpendicular magnetic field  $B$  such that a voltage  $V$  is measured in the transverse direction.

plateaus were given by the formula  $R_H = \frac{1}{\nu} \cdot \frac{h}{e^2}$ , where  $\nu$  is an integer. In addition, at the magnetic fields where the plateaus appeared in the Hall resistance, the longitudinal resistance  $R_{\parallel}$  dropped to zero. This new phenomena was dubbed the Integer Quantum Hall Effect (IQHE). The IQHE is that precise that it effectively defines the unit of resistance. The fundamental unit of resistance can be measured with an accuracy of  $10^{-12}$  to be  $R_K = \frac{h}{e^2} = 25812.807557(18) \Omega$ [30].

As samples became cleaner, and temperatures lower, new features appeared in the resistance spectrum. New plateaus were observed, together with dips in the longitudinal resistivity. These new plateaus were located at  $R_H = \frac{1}{\nu} \cdot \frac{h}{e^2}$ , where  $\nu = \frac{p}{q}$  formed fractions, such as  $\frac{1}{3}$ ,  $\frac{2}{5}$  and  $\frac{3}{7}$ . The plateaus only developed at fractions with an odd denominator, as can be seen in Figure 2.2. The new effect was named Fractional Quantum Hall Effect (FQHE). Compared to the IQHE it has more features beyond simply a fractional Hall resistance. One prominent feature is that the minimal excitations do not consist of individual electrons but rather of fractionally charged quasi-particles[18], that do not obey the ordinary statistics of fermions or bosons. This new form of statistics constitutes a generalization of the fermion/boson statistics and can only be obtained in systems with lower dimensionality than 3. Some of these quasi-particles even display non-abelian statistics[20], in theory. The experimental verification of the non-abelian statistics is still lacking, but this is the reason that people are looking to FQHE as a means of building a quantum computer.

The key to understanding the IQHE lies in the behaviour of single particles in a magnetic field. From classical physics we know that charged particles are deflected by magnetic fields and therefore move in circles where the radius is proportional to the particle's momentum. The frequency of revolution is therefore independent of the particle momentum. It depends only on the magnetic field  $B$  and on the mass  $m$  of the particle, as expressed by the formula  $\omega_c = \frac{eB}{mc}$ . The oscillatory behaviour is similar to the behaviour of the Harmonic Oscillator, where the quantum mechanical energy levels are equally spaced as  $E_n = \hbar\omega \left(n + \frac{1}{2}\right)$  with  $n$  being an integer. An analogous calculation for a particle in a magnetic field shows that here, too, the energy levels are equally spaced, with  $E_n = \hbar\omega_c \left(n + \frac{1}{2}\right)$ . Each energy level is called a Landau Level (LL), after Landau[16] who solved the problem in 1930. The LL with  $n = 0$  is the minimum energy level and therefore called the Lowest Landau Level (LLL). In contrast to the Harmonic Oscillator, each LL is massively degenerate, as there exists one state for each



### 2.3 The Laughlin Construction and the Hierarchy

In 1983 Robert Laughlin proposed a wave function that would explain the FQHE at  $\nu = \frac{1}{q}$ , where  $q$  is an odd integer[18]. The construction was inspired by the realization that in the FQH-states the electrons could minimize their interaction energy by being as far from each other as possible. With that as a guiding star, he proposed the now famous wave function

$$\Psi_{\frac{1}{q}}(z_1, \dots, z_{N_e}) = e^{-\frac{1}{4} \sum_j |z_j|^2} \prod_{i < j}^{N_e} (z_i - z_j)^q, \quad (2.1)$$

which is a homogeneous state with well-defined angular momentum. This wave function implied that only odd denominator filling fractions could appear, since otherwise the wave function would not be antisymmetric in the electron coordinates. Starting from (2.1) he could also find the elementary excitations, also called quasi-particles, that could appear. This was accomplished by inserting an extra quantum of flux into the state at  $z = \eta$ , and noting that the new wave function contained an extra factor  $\prod_j (z_j - \eta)$ . By making an analogy with a charged plasma, Laughlin could deduce that the quasi-particles at  $\nu = \frac{1}{q}$  have fractional charges  $\frac{e}{q}$ . The physical picture is that the term  $(z - \eta)$  does not repel the electron and quasi-particle as strongly as the  $(z_i - z_j)^q$  repels the electrons from each other. This gives the quasi-particle a smaller correlation hole than the electron. Later Arovas, Schrieffer and Wilczek deduced that the quasi-particles have fractional exchange statistics[1].

The Laughlin wave function sheds some light on other filling fractions as well, since the quasi-particle excitations can be used as building blocks for other states. As the magnetic field  $B$  is tuned away from  $\nu = \frac{1}{q}$ , quasi-particles appear in the state (2.1). As  $B$  is tuned still further, these quasi-particles become so numerous that the electrons and quasi-particles condense into a new state, with a new filling fraction. This new state will also support its own quasi-particles with fractional charges and statistics. These 2<sup>nd</sup> level quasi-particles can in turn, as the magnetic field is changed further, condense into yet another state. By this process any filling fraction with an odd denominator can be created by continuous condensation of parent quasi-particles[7, 11]. This idea is called the Haldane-Halperin hierarchy construction, since different filling fractions come at different hierarchical levels of condensation of quasi-particles.

Each level of the hierarchy has both negatively and positively charged quasi-particles. The negatively\* charged excitations are called quasi-holes. Depending on if quasi-particles or quasi-holes are condensed, different technical issues arise. Usually quasi-particle condensation is more simple and quasi-hole condensation more difficult.

In the hierarchy, all quasi-particle excitations are gapped, compared to the ground state. This gap sheds some light in which order the different fractions should become visible in experiments. If the FQHE is to be measured, it is important that the gap to quasi-particle excitation is not bridged by temperature or impurities. It can be shown, under certain circumstances, that the excitation gap of the FQHE at  $\nu = \frac{p}{q}$  is monotonically vanishing in  $q$ [3]. This explains why the fractions at  $\nu = \frac{1}{3}$  and  $\nu = \frac{2}{3}$  are observed first, followed by the fractional at  $\nu = \frac{2}{5}$ ,  $\nu = \frac{3}{7}$  and  $\nu = \frac{4}{9}$  etc.

### 2.4 Composite Fermions

A different route to explaining the FQHE was taken by Jain. Inspired by Laughlin's wave function and resistance measurements, he unified the FQHE and the IQHE by introducing

---

\*Negative charge with respect to the electron charge.

the notion of composite fermions[13]. Jain proposed that the electrons could screen parts of the magnetic field by binding vortices to themselves. By binding just enough vortices, which reduces the magnetic field, the electrons would fill one or more effective LLs. This construction yielded explicit expressions for wave functions at other filling fractions than  $\nu = \frac{1}{q}$ , something that the hierarchy construction could not achieve. Furthermore, Jain found that the wave functions for Composite Fermions also displayed remarkably good overlap, with those obtained from exact diagonalization of the Coulomb potential.

There now exists an alternative method for deducing trial wave functions for generic FQH-states, based on the similarity between the Laughlin wave function and correlators in Conformal Field Theory (CFT). These CFT-based wave functions, reproduce the wave functions deduced using the composite fermion picture. Thus the composite fermion scheme can be seen as a special case of the hierarchy construction and implies that these two approaches are two alternative ways of looking at the same problem.

## 2.5 Fractional Quantum Hall Effect on a Torus

In this licentiate thesis we will consider the Haldane-Halperin hierarchy wave functions in a toroidal geometry. By construction, the torus lacks a boundary, making it suitable for numerical calculations. The torus is also locally flat, which avoids the trouble that is connected to the curved space of the sphere – another geometry that lacks boundaries. Further, the number of states in the torus Hilbert space is the same as the number of magnetic flux quanta  $N_s = \frac{A}{2\pi\ell^2}$ , where  $A$  is the torus area.

The torus does of course come with its own set of problems. Because of the periodicity, wave functions expressed on the torus have rather complicated analytical forms. This includes products of Jacobi  $\vartheta$ -functions  $\vartheta_j(z|\tau)$ , making analytical manipulations more complicated. Also because of the gauge field associated with the magnetic field, the wave functions are not truly periodic, as there is a restriction on which translation operators that are allowed on the torus.

Examining this restriction will form a central part of this thesis. This is an interesting problem, as this restriction prohibits the mapping of CFT wave functions formulated on the plane directly to the torus. Technically this is because the planar wave functions in the higher levels of the Haldane-Halperin hierarchy will contain derivative operators  $\partial_z$ . We will later show that these derivatives can *not* be interpreted as derivatives on the torus. Instead the derivative can, at best, be mapped onto a linear combination of allowed translation operators  $t_x$  as  $\partial_z \rightarrow \sum_l a_l t_x^l$ . The precise meaning of derivatives and translation operators will be clarified in Section 3.3 and 4.2.1.

## Chapter 3

# Coherent States in a Magnetic Field

Coherent states can be thought of as the quantum mechanical analogue of classical states. There are several ways of defining coherent states, but in the simplest cases they are maximally localized in phase space. The coherent states also obey the classical equations of motion.

In order to set the stage for coherent states on torus, we will review the concept of coherent states in general. As a warm-up, and to set the notation, we will construct the coherent states in the Harmonic Oscillator. We will then construct coherent states in a magnetic field on the plane. After that we will explain why the torus poses a problem and why the methods we employed, for the Harmonic Oscillator and on the plane, cannot be directly applied to the torus. Finally we will then construct two candidates for coherent states on the torus and analyse their properties.

We will in several sections characterize the states with the use of the Heisenberg uncertainty relation. We therefore review its general form and basic properties. The general form of the uncertainty relations states that

$$\sigma_A \sigma_B \geq \frac{1}{2} |\langle [A, B] \rangle|. \quad (3.1)$$

We define the uncertainty  $\sigma_A$  of an operator  $A$  as  $\sigma_A^2 = \langle A^2 \rangle - \langle A \rangle^2$ , where  $\langle \mathcal{O} \rangle$  is an expectation value with respect to the operator  $\mathcal{O}$  for a specific state. In the special case where of  $\hat{x}$  and  $\hat{p}$  the relation (3.1) reduces to  $\sigma_x \sigma_p \geq \frac{1}{2} \hbar$  since  $[x, p] = i\hbar$  is just a complex number.

### 3.1 Coherent States in the Harmonic Oscillator

We begin by reviewing the coherent states in the Harmonic Oscillator. The one-dimensional quantum Harmonic Oscillator has a Hamiltonian  $H = \frac{1}{2m} \hat{p}^2 + m\omega^2 \hat{x}^2$ . Using a suitable choice of variables, we may rewrite this  $H$  as  $H = \hbar\omega (a^\dagger a + \frac{1}{2})$ , where

$$a = \sqrt{\frac{m\omega}{2\hbar}} \left( \hat{x} + \frac{i}{m\omega} \hat{p} \right) \quad (3.2)$$

$$a^\dagger = \sqrt{\frac{m\omega}{2\hbar}} \left( \hat{x} - \frac{i}{m\omega} \hat{p} \right) \quad (3.3)$$

and  $[a, a^\dagger] = 1$ . A complete basis of solutions is given by the states that are eigenstates of  $a^\dagger a$ , such that  $a^\dagger a |n\rangle = n |n\rangle$ . We seek states that fulfil the equality in Heisenberg's uncertainty relation  $\sigma_x \sigma_p \geq \frac{\hbar}{2}$ , and start by examining the states  $|n\rangle$ . For this calculation,  $\hat{x}$  and  $\hat{p}$  are

expressed in terms of  $a$  and  $a^\dagger$  as

$$\hat{x} = \sqrt{\frac{\hbar}{2m\omega}} (a^\dagger + a) \quad (3.4)$$

$$\hat{p} = i\sqrt{\frac{m\omega\hbar}{2}} (a^\dagger - a). \quad (3.5)$$

For the state  $|n\rangle$ , it is straightforward to verify that  $\langle n|\hat{x}|n\rangle = \langle n|\hat{p}|n\rangle = 0$ . It is also simple to show that  $\langle n|\hat{x}^2|n\rangle = \frac{\hbar}{m\omega} (n + \frac{1}{2})$  and that  $\langle n|\hat{p}^2|n\rangle = m\omega\hbar (n + \frac{1}{2})$ . Putting all the pieces together the result is  $\sigma_x\sigma_p = \hbar (n + \frac{1}{2})$ . It is only the state  $|0\rangle$  that equates the uncertainty relation, and this happens to be an eigenstate of the  $a$  operator with eigenvalue 0. We may thus instead look for the eigenstates of  $a$  and  $a^\dagger$ . It is simple to verify that there are no eigenstates of  $a^\dagger$ . The class of states that are eigenstates of  $a$  are characterized by a complex number  $\alpha$  such that  $a|\alpha\rangle = \alpha|\alpha\rangle$  and  $\langle\alpha|a^\dagger = \langle\alpha|\alpha$ . These normalized states are the Coherent States (CS)

$$|\alpha\rangle = e^{-\frac{1}{2}|\alpha|^2} e^{\alpha a^\dagger} |0\rangle = e^{\alpha a^\dagger + \alpha^* a} |0\rangle. \quad (3.6)$$

The states  $|\alpha\rangle$  are not energy eigenstates but are instead maximally localized in phase space. From (3.4) and (3.5) it is easy to see that the state  $|\alpha\rangle$  has  $\langle x\rangle = \sqrt{\frac{2\hbar}{m\omega}} \Re(\alpha)$  and  $\langle p\rangle = \sqrt{2m\omega\hbar} \Im(\alpha)$  as well as  $\langle x^2\rangle = \frac{2\hbar}{m\omega} \left[ \Re(\alpha)^2 + \frac{1}{4} \right]$  and  $\langle p^2\rangle = 2m\omega\hbar \left[ \Im(\alpha)^2 + \frac{1}{4} \right]$ . This shows that these states indeed minimize  $\sigma_x\sigma_p$  since the variance is  $\sigma_x^2 = \langle x^2\rangle - \langle x\rangle^2 = \frac{\hbar}{2m\omega}$  and  $\sigma_p^2 = \frac{1}{2}m\omega\hbar$  which gives the product  $\sigma_x\sigma_p = \frac{\hbar}{2}$ . Note that  $\alpha = 0$  corresponds to the ground state  $|0\rangle$  which is of course annihilated by  $a$ .

The states  $|\alpha\rangle$  do not only saturate the Heisenberg uncertainty relations, they also possess a time evolution that mimics that of a classical particle. We know from the commutation relations that  $\langle x\rangle = \frac{1}{m} \langle p\rangle$  and  $\langle \dot{p}\rangle = -m\omega^2 \langle x\rangle$  such that the time evolution of  $|\alpha\rangle$  is  $|\alpha_0 e^{i\omega t + i\phi}\rangle$  with energy  $\langle E\rangle_\alpha = \hbar\omega \left( |\alpha_0|^2 + \frac{1}{2} \right)$ . These states are therefore moving on circles in phase space with expectation value  $\langle x\rangle = x_{\max} \cos(\omega t + \phi)$  where  $x_{\max} = \sqrt{\frac{2\hbar}{m\omega}} |\alpha_0|$ . As these states are *not* energy eigenstates, the uncertainty in energy  $\sigma_E = \sqrt{\langle E^2\rangle_\alpha - \langle E\rangle_\alpha^2}$  is finite, and equal to  $\sigma_E = \hbar\omega |\alpha_0|$ .

## 3.2 Coherent States in a Magnetic Field in Planar Geometry

In the previous section we saw that we could construct coherent states in the Harmonic Oscillator as eigenstates of the ladder operators. On a plane in a magnetic field, a similar thing happens, but with two operators instead of one. The Hamiltonian for a particle in a magnetic field is given by

$$\hat{H} = \frac{1}{2m} (p_y - eA_y)^2 + \frac{1}{2m} (p_x - eA_x)^2 \quad (3.7)$$

where  $\mathbf{A} = (A_x, A_y, A_z)$  is a vector potential such that  $\mathbf{B} = \nabla \times \mathbf{A}$ . Depending on the choice of gauge, we may introduce suitable ladder operators such that the Hamiltonian can again be written as  $\hat{H} = \hbar\omega (a^\dagger a + \frac{1}{2})$ . Here there are two dimensions,  $x$  and  $y$ , so we may now construct two kinds of ladder operators instead of one. One set of operators are  $a$  and  $a^\dagger$ , which step up and down in what we call Landau levels. These operators change the energy of the

state, just like the ladder operators in the Harmonic Oscillator. The other set of operators is  $b$  and  $b^\dagger$  which, in symmetric gauge, change the angular momentum of the electron. These operators keep the electrons within a given Landau level\* and are thus responsible for the large degeneracy within each LL. The operators have the usual ladder operator commutation relations  $[a, a^\dagger] = [b, b^\dagger] = 1$  and  $[a, b] = [a, b^\dagger] = 0$ . Using these, we may construct the eigenstates of  $a$  and  $b$  such that  $a|\alpha, \beta\rangle = \alpha|\alpha, \beta\rangle$  and  $b|\alpha, \beta\rangle = \beta|\alpha, \beta\rangle$ . In analogy with the Harmonic Oscillator, these states can be expressed as

$$|\alpha, \beta\rangle = e^{-\frac{1}{4}|\alpha|^2 - \frac{1}{4}|\beta|^2} e^{\frac{1}{\sqrt{2}}(\alpha a^\dagger + \beta b^\dagger)} |0\rangle \quad (3.8)$$

where an extra factor of  $\frac{1}{\sqrt{2}}$  has been introduced for later convenience. The state  $|0\rangle$  is destroyed by both  $a$  and  $b$ . The Hamiltonian can be written as  $\hat{H} = \hbar\omega (a^\dagger a + \frac{1}{2})$  which means that  $\alpha$  must be related to the orbital motion of the electron whereas  $\beta$  must be related to the guiding centre of the motion.

Let us quantify this. In symmetric gauge,  $\mathbf{A} = \frac{1}{2}B(y\hat{x} - x\hat{y})$ , the ladder operators are given as

$$\begin{aligned} a &= \frac{1}{\sqrt{2}} \left( \frac{\bar{z}}{2} + 2\partial_z \right) & b &= \frac{1}{\sqrt{2}} \left( \frac{z}{2} + 2\partial_{\bar{z}} \right) \\ a^\dagger &= \frac{1}{\sqrt{2}} \left( \frac{z}{2} - 2\partial_{\bar{z}} \right) & b^\dagger &= \frac{1}{\sqrt{2}} \left( \frac{\bar{z}}{2} - 2\partial_z \right) \end{aligned}$$

where all the dimensional factors have been suppressed since we set  $\hbar = \omega = m = 1$ . We have also introduced complex coordinates as  $z = x + iy$ . Inverting the relations above means that the coordinate and momentum operators can be expressed in terms of  $a$  and  $b$  as

$$\begin{aligned} z &= \sqrt{2} (b + a^\dagger) & \partial_z &= \frac{1}{2\sqrt{2}} (a - b^\dagger) \\ \bar{z} &= \sqrt{2} (a + b^\dagger) & \partial_{\bar{z}} &= \frac{1}{2\sqrt{2}} (b - a^\dagger). \end{aligned}$$

We immediately see that the positions expectation value for the coherent states is  $\langle z \rangle = (\beta + \bar{\alpha})$ . Calculating the time evolution of  $\langle z \rangle$ , we get  $\langle \dot{z} \rangle = \langle \frac{-i}{\hbar} [z, H] \rangle = i\omega\bar{\alpha}$  giving the solution  $\langle z \rangle = (\beta + \alpha_0 e^{i\omega t + i\phi_0})$ . We may interpret this as the electron circulating at a radius  $\alpha_0$  around a guiding centre  $\beta_0$  with a frequency of  $\omega$ . This state has energy  $\langle E \rangle_{\alpha, \beta} = H = \hbar\omega \left( \frac{1}{2} |\alpha_0|^2 + \frac{1}{2} \right)$ .

A different way of looking at (3.8) is to first create a coherent excitation centred at  $z = 0$  using  $e^{-\frac{1}{4}|\alpha|^2} e^{\frac{1}{\sqrt{2}}\alpha a^\dagger}$ , and then move to  $z = \beta$  by  $e^{-\frac{1}{4}|\beta|^2} e^{\frac{1}{\sqrt{2}}\beta b^\dagger}$ . The operator  $e^{\beta b^\dagger - \bar{\beta} b}$  can be interpreted as a translation operator  $t(\beta)$  that moves a wave function a distance  $\beta$  without changing its energy. This point of view will be fruitful in understanding why  $b$  and  $b^\dagger$  fail to be good operators on the cylinder and torus.

Comparing with the Harmonic Oscillator, the coherent state  $|\alpha, \beta\rangle$  now precess in real space whereas the Harmonic Oscillator state precesses in phase space. We may thus think of the real space probability distribution  $|\langle z | \alpha, \beta \rangle|^2$  in a magnetic field, in analogy to the phase space quasi-probability distribution of the Harmonic Oscillator[25], even though the concepts are not mathematically equivalent. An important difference is that in the Harmonic Oscillator all states

---

\*Since neither  $b$  nor  $b^\dagger$  appear in the Hamiltonian these operators map out a degenerate subspace in each Landau level.



circulate around  $\langle x \rangle = \langle p \rangle = 0$ , whereas in the magnetic field the coherent states may circulate around any point  $\langle z \rangle = \beta$ . This difference introduces an extra degree of freedom, which will affect the uncertainty relations (3.1). One special uncertainty relation that will be modified, is between  $x$  and  $y$ , within a given LL. Because of the vector potential,  $y$  will play the role of  $p$ , with the existence of the magnetic field. In terms of ladder operators, the positions operators are

$$\begin{aligned}\hat{x} &= \frac{\ell}{\sqrt{2}} (a + b + a^\dagger + b^\dagger) \\ \hat{y} &= \frac{\ell}{i\sqrt{2}} (b + a^\dagger - a - b^\dagger).\end{aligned}$$

Within the LLL we define the projected operators as

$$\begin{aligned}\hat{x}_{\text{LLL}} &= \mathcal{P}_{\text{LLL}} \hat{x} \mathcal{P}_{\text{LLL}} = \frac{\ell}{\sqrt{2}} (b + b^\dagger) \\ \hat{y}_{\text{LLL}} &= \mathcal{P}_{\text{LLL}} \hat{y} \mathcal{P}_{\text{LLL}} = \frac{\ell}{i\sqrt{2}} (b - b^\dagger),\end{aligned}$$

and these do not commute,  $[\hat{x}_{\text{LLL}}, \hat{y}_{\text{LLL}}] = i\ell^2$ . Thus the product  $\sigma_x \sigma_y$  will be calculated repeatedly in the coming sections. We will call this measure the *delocalization*, since  $\sigma_x \sigma_y$  is a measure of the occupied area of a state. The minimal  $\sigma_x \sigma_y$  delocalization within a LL will however not be  $\frac{\ell^2}{2}$  as we would have expected from the analogy with the Harmonic Oscillator. Instead it will be  $\ell^2$ , since now there exists two ladder operators that contribute to both the  $x$  and  $y$  operators. The easy way to see this is that  $\sigma_x^2 = \langle x^2 \rangle - \langle x \rangle^2$  is different from  $\sigma_{x_{\text{LLL}}}^2 = \langle x_{\text{LLL}}^2 \rangle - \langle x_{\text{LLL}} \rangle^2$ , even within a single LL.

Indeed we see for the coherent states, that  $\langle x \rangle = \Re(\beta + \alpha)$  and  $\langle y \rangle = \Im(\beta - \alpha)$  and  $\langle x^2 \rangle = \Re^2(\alpha + \beta) + 1$  as well as  $\langle y^2 \rangle = \Im^2(\beta - \alpha) + 1$ . Thus when we restore units  $\sigma_x \sigma_y = \ell^2$  and these states saturate the Heisenberg uncertainty relation. The states  $|0, \beta\rangle$  are energy eigenstates since  $b$  and  $b^\dagger$  are not present in the Hamiltonian. These states are thus stationary under time evolution and represent localized LLL particles. In fact, the state  $|0, \beta\rangle$  can be obtained by projecting a spacial delta function  $\delta^{(2)}(z - \beta)$  onto the LLL such that  $\langle z | 0, \beta \rangle = \mathcal{P}_{\text{LLL}} \delta^{(2)}(z - \beta)$ .

On the torus, we would like to perform the same construction as on the plane, and find localized states within the LLL. Unfortunately there are no analogues of the  $b$  or  $b^\dagger$  operators here since we break the rotational invariance. Under this change of geometry, the  $b$  and  $b^\dagger$  operators are replaced by translation operators  $t_x$  and  $t_y$ . These operators have different commutation relations than  $b$ ,  $b^\dagger$ . A consequence of this problem is that  $\langle z \rangle$  is no longer well-defined, as it will depend on how the torus is parametrized. In fact, already the cylinder poses a problem, as it has periodic boundary conditions in one direction. Going to the torus only makes matters worse. In essence, since rotational invariance is broken down to translational invariance, another basis needs to be found. On the cylinder the basis of choice is a linear basis, which respects the geometry of the cylinder. These states are plane waves in one direction and localized Gaussians in the other. Unfortunately there is no natural highest weight state, *i.e.* there is no state  $|0\rangle$  from which all other states can be generated, and which is annihilated by the conjugate operator. We will clarify this as we more thoroughly define the torus.

If we cannot use the ladder operators, then what strategy can we use? We choose to project a spacial delta function onto the LLL as a means to construct coherent states on the toroidal geometry. Our hope is that  $\mathcal{P}_{\text{LLL}} \delta^{(2)}(z - z')$  gives a state that is analogous to  $\alpha = 0$  and  $\beta = z'$ . We will also explore an alternative method of explicitly constructing a family of coherent states.

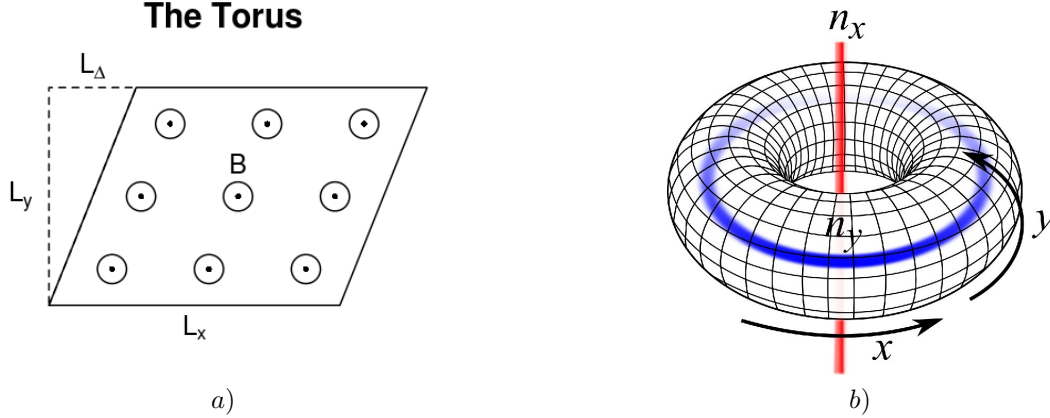


Figure 3.1: a) The toroidal geometry: Width  $L_x$ , height  $L_y$ , skewness  $L_\Delta$ . All points on the lattice  $\mathbf{r} = n\mathbf{L}_1 + m\mathbf{L}_2 = (nL_x + mL_\Delta)\hat{\mathbf{x}} + mL_y\hat{\mathbf{y}}$  are identified. b) Changing the boundary conditions is equivalent to inserting fluxes through the two cycles of the torus. As fluxes  $n_x$  and  $n_y$  are inserted, the positions of all the states are transported along the principal directions of the torus. Changing the boundary conditions by  $2\pi$  is equivalent to adding one unit of flux.

### 3.3 The Torus Itself

So what do we mean by a torus? In simple words, a torus is a surface that has periodic boundary conditions in two directions. We can think of the torus as a doughnut, such as the one depicted in the right panel of Figure 3.1, although we should remember that our torus is locally flat.

Mathematically the torus is characterized by two lattice vectors  $\mathbf{L}_1 = L_x\hat{\mathbf{x}}$  and  $\mathbf{L}_2 = L_\Delta\hat{\mathbf{x}} + L_y\hat{\mathbf{y}}$  and this geometry is depicted in the left panel of Figure 3.1. We should think of  $L_x$  and  $L_y$  as the width and height of the torus respectively whereas  $L_\Delta$  is the skewed distance of the torus. Through the surface there is a magnetic field pointing in the  $\hat{\mathbf{z}}$ -direction,  $\mathbf{B} = B\hat{\mathbf{z}}$ . To describe the magnetic field we will use the Landau gauge  $\mathbf{A} = -By\hat{\mathbf{x}}$  such that  $\mathbf{B} = \nabla \times \mathbf{A}$ .

The single particle Hamiltonian on the torus is still given by (3.7), and we seek a set of operators that commute with  $H$ , and can translate a wave function a distance  $\mathbf{L}$ . For the free Hamiltonian  $H_{\text{free}} = \frac{\mathbf{p}^2}{2m}$ , this operator is the ordinary  $t_{\text{free}}(\mathbf{L}) = e^{\mathbf{L} \cdot \nabla}$ , that has the effect  $t_{\text{free}}(\mathbf{L})\psi(\mathbf{x}) = \psi(\mathbf{x} + \mathbf{L})$ . In a magnetic field  $[H, t_{\text{free}}] \neq 0$ , so the operator  $t(\mathbf{L})$  that translates a wave function in some direction  $\mathbf{L}$  is more complicated than if there was no magnetic field present. In our specific gauge, the operator is written as

$$t(\mathbf{L}) = \exp \left[ \mathbf{L} \cdot \nabla + \frac{1}{\ell^2} \{ \mathbf{L} \cdot y\hat{\mathbf{x}} - i\hat{\mathbf{z}} \cdot (\mathbf{L} \times \mathbf{r}) \} \right], \quad (3.9)$$

where for clarity the magnetic length  $\ell$  has been restored. The first part of  $t(\mathbf{L})$  is the same as for the free Hamiltonian. The second part of  $t(\mathbf{L})$  encodes the gauge transformation needed to commute with  $H$ . When convenient, the complex notation  $t(\alpha + i\beta) \equiv t(\alpha\hat{\mathbf{x}} + \beta\hat{\mathbf{y}})$  will be used, and the magnetic length  $\ell$  will be set to  $\ell = 1$ . For translations in the  $x$  and  $y$  directions, we may evaluate the effect of the translation operator as  $t(\alpha\hat{\mathbf{x}})f(x, y) = f(x + \alpha, y)$  and  $t(\beta\hat{\mathbf{y}})f(x, y) = e^{i\beta x}f(x, y + \beta)$ . Just as  $\hat{x}$  and  $\hat{y}$  did not commute on the plane, neither do translations in different directions. We rather have a magnetic algebra

$$t(\gamma)t(\delta) = t(\delta)t(\gamma)e^{\frac{i}{2\ell^2}\Im(\gamma\bar{\delta})}, \quad (3.10)$$

such that when translating around a closed loop, we pick up a phase equal to the area enclosed by the loop. Since the torus has a closed surface, and there should be no ambiguity in the phase depending on which side of the loop we choose as the interior, there are constraints on the area of the torus. Requiring single-valued wave functions in this way, we find the area of the torus to be  $L_x L_y = 2\pi N_s$ , where  $N_s$  is an integer equal to the number of flux quanta that pierce the torus. We can thus express  $L_x$ ,  $L_y$  and  $L_\Delta$  in terms of the complex modular parameter  $\tau = \frac{1}{L_x} (L_\Delta + iL_y)$  and  $N_s$ .

The periodic boundary conditions are implemented as

$$t(L_x) \psi(z) = e^{i\phi_1} \psi(z) \quad (3.11)$$

$$t(\tau L_x) \psi(z) = e^{i\phi_2} \psi(z), \quad (3.12)$$

where the phase angles  $\phi_i$  have the physical interpretation of fluxes threading the two cycles of the torus. The interpretation is illustrated in Figure 3.1b. The physical effects of changing  $\phi_j$  is that all states on the torus will shift their positions. By letting  $\phi_j \rightarrow \phi_j + 2\pi$ , each state will have transformed into another state a short distance away.

We now see why the  $b$  and  $b^\dagger$  operators are not useful on the cylinder and the torus. Imposing periodic boundary conditions requires that all operators have to commute with  $t(L_x)$  on the cylinder and also  $t(\tau L_x)$  on the torus. Since the commutator  $[t(L_x), b] = L_x t(L_x)$  and  $[t(L_x), b^\dagger] = L_x t(L_x)$  are not zero, we find that only the combination  $b - b^\dagger$  is allowed on the cylinder. Adding the torus constraint and  $[t(\tau L_x), b] = \tau L_x t(\tau L_x)$ ,  $[t(\tau L_x), b^\dagger] = \bar{\tau} L_x t(\tau L_x)$ , we find that no linear combination of  $b$  and  $b^\dagger$  is allowed on the torus\*.

As a direct consequence of the imposed boundary conditions on the torus, not all vectors  $\mathbf{L}$  are valid in the translation operator  $t(\mathbf{L})$ . If we wish to stay within a specific sector of boundary conditions, then by necessity  $[t(\mathbf{L}), t(L_x)] = [t(\mathbf{L}), t(\tau L_x)] = 0$ . Only a subset of  $t(\mathbf{L})$  satisfy this condition. These translation vectors fall on the lattice  $\Gamma = \frac{L_x}{N_s} n + \frac{L_x}{N_s} \tau m$  for integers  $n$  and  $m$ . The existence of this sub-lattice necessitates the introduction of the notation

$$x_n = n \frac{L_x}{N_s} \quad y_n = n \frac{L_y}{N_s} \quad \omega_n = n \frac{L_\Delta}{N_s}. \quad (3.13)$$

Equation (3.13) parametrizes the natural sub-lattice formed by these translations, that preserve the boundary conditions. The two operators that map out this lattice are

$$t_1^n \equiv t(x_n) \quad (3.14)$$

$$t_2^m \equiv t(\tau x_m) = t(\omega_m + i y_m), \quad (3.15)$$

which translate in the two main directions on the sub-lattice. In the following we shall fix the boundary conditions to  $\phi_1 = \phi_2 = 0$ . It is at any time possible to restore the generic periodic boundary conditions of  $\phi_1$  and  $\phi_2$  by acting with  $t(\gamma)$ , where  $\gamma = (\phi_1 \tau - \phi_2) \frac{1}{L_y}$ .

### 3.4 Basis states

In the Landau gauge described above, the Hamiltonian for a charged particle in a magnetic field is expressed as

$$\hat{H} = \frac{1}{2m} p_y^2 + \frac{1}{2m} (p_x - eBy)^2. \quad (3.16)$$

---

\*In the special case of  $\Im(\tau) = 0$  the  $b - b^\dagger$  operator is still allowed, but then  $\tau L_x$  and  $L_x$  are linearly dependant.

On the cylinder, the normalized eigenstates with energy  $E_n = \hbar\omega \left(n + \frac{1}{2}\right)$  of this Hamiltonian are given by

$$\chi_{n,s}(x, y) = \frac{1}{\sqrt{L_x}\sqrt{\pi}} e^{-iy_s x} H_n(y - y_s) e^{-\frac{1}{2}(y - y_s)^2} \quad (3.17)$$

where  $H_n$  is an Hermite polynomial. It is easy to see that  $t_2^m \chi_{n,s} = t(y_m \hat{\mathbf{y}}) \chi_{n,s} = \chi_{n,s-m}$  so there is no lowest-weight state fulfilling  $t_2^{-1} \chi_{n,s} = 0$ . Since the cylinder has an infinite amount of basis states for both positive and negative  $s$  the bottom will never be reached by the application of  $t_2$ .

Going from the cylinder to the torus, we must periodize  $\chi_{n,s}$  in the  $\mathbf{L}_2$ -direction, as the cylinder functions are only periodic in the  $\mathbf{L}_1$ -direction. We achieve this by construction the torus wave function  $\eta_{n,s}$ , as a linear combination of the states  $\chi_{n,s+kN_s}$ ,  $k \in \mathbb{Z}$ . The LLL basis wave functions on the torus are

$$\eta_s(z) = \frac{1}{\sqrt{L_x}\sqrt{\pi}} \sum_t e^{i\frac{1}{2}(y_s + tL_y)(\omega_s + tL_\Delta)} e^{-i(y_s + tL_y)x} e^{-\frac{1}{2}(y - y_s - tL_y)^2}. \quad (3.18)$$

This may be rewritten as

$$\eta_s(z) = \frac{e^{-\frac{1}{2}y^2}}{\sqrt{L_x}\sqrt{\pi}} \vartheta \left[ \begin{matrix} -\frac{s}{N_s} \\ 0 \end{matrix} \right] \left( \frac{N_s}{L_x} z \middle| N_s \tau \right). \quad (3.19)$$

In equation (3.19), the generalized quasi-periodic Jacobi  $\vartheta$ -function is introduced. (The definition of  $\vartheta$  is found in equation (A.1) in the Appendix, which contains a collection of useful formulae related to the Jacobi  $\vartheta$ -functions.) From (3.19) it is easy to see that there are  $N_s$  linearly independent basis states, as  $\eta_{s+N_s} = \eta_s$ .

The basis  $\eta_s$  consists of eigenfunctions of  $t_1$ , but it is also possible to construct eigenfunctions of  $t_2$  instead. Since we know that the phase that accompanies commutation of  $t_1^n$  and  $t_2^s$  is  $e^{ix_n y_s}$ , the eigenfunctions of  $t_2$  can formally be written as  $\varphi_l(z) = \frac{1}{\sqrt{N_s}} \sum_s e^{-ix_l y_s} \eta_s(z)$ . Using a transformation property of the  $\vartheta$ -function under Fourier sums, (A.9), the eigenfunctions of  $t_2$  can immediately be expressed as

$$\varphi_l(z) = \frac{e^{-\frac{1}{2}y^2}}{\sqrt{N_s L_x} \sqrt{\pi}} \vartheta \left[ \begin{matrix} 0 \\ \frac{l}{N_s} \end{matrix} \right] \left( \frac{1}{L_x} z \middle| \frac{\tau}{N_s} \right). \quad (3.20)$$

A more physical approach to constructing  $\varphi_l$  can be taken by noticing that all the physics should be invariant under the identification  $\mathbf{L}_1 \rightarrow \mathbf{L}_2$  and  $\mathbf{L}_2 \rightarrow -\mathbf{L}_1$ . This is equivalent to a rotation of the coordinate system. Seen from this point of view  $\varphi_l$  can be obtained from  $\eta_s$  without the need to explicitly utilize the Fourier summation. This is done by performing the modular transformation  $\tau \rightarrow -\frac{1}{\tau}$ , while letting  $z \rightarrow \frac{|\tau|}{\tau} z$ , and applying the appropriate gauge transformation connected with the rotation described above.

### 3.5 Lattice Coherent States (LCS)

An interesting feature of the LLL is that all states in this level can be written as a Gaussian factor  $e^{-\frac{1}{2}y^2}$  times a holomorphic function  $\rho(z)$ . Since the torus has periodic boundary conditions and  $\rho(z)$  is holomorphic, then  $\rho(z)$  must contain some zeroes, as it would otherwise be constant. As a consequence of being holomorphic, the function  $\rho(z)$  is also fully determined by the location of these zeroes. We may thus fully characterize any LLL wave functions by the location of

its zeroes. By choosing these zeroes appropriately, this may allow us, at least in principle, to engineer states with some desired properties.

In 1985 Haldane and Rezayi proposed a candidate for a localized wave function. They did so by putting all zeros at the same point[9]. A wave function with  $N_s$  fluxes has  $N_s$  zeroes in the principle domain, corresponding to the  $N_s$  linearly independent basis states at that flux. By fixing the boundary conditions of the wave function, constraints on the locations of the zeroes are introduced, such that there are only  $N_s^2$  points where the  $N_s$ -fold zeros can be. Each of the  $N_s^2$  points corresponds to a wave function. Since the LLL only can hold  $N_s$  linearly independent states the proposed states must be linearly dependent and over-complete. Over-completeness is nothing troublesome in itself and we have encountered it before, both in the Harmonic Oscillator and as well in the magnetic field on the plane. This particular set of states, we shall refer to as, Lattice Coherent States (LCS). As shall be seen later, it is strictly speaking only in a region around  $\Re(\tau) = 0$  that these states can be considered localized. As  $\tau \rightarrow \tau + \frac{1}{2}$ , the LCS goes through a transition from one localized maxima to two well separated maxima. On a rectangular ( $\Re(\tau) = 0$ ) torus, the LCS do approach the expected limit  $\sigma_x \sigma_y = 1$  as  $N_s \rightarrow \infty$ . Hence in the thermodynamic limit, the LCS are likely to be identical to the coherent states on the plane.

The construction of the LCS rests on the observation that a general wave function in the LLL on a torus can be written as

$$\psi(z) = \mathcal{N} e^{-\frac{y^2}{2}} e^{ikz} \prod_{j=1}^{N_s} \vartheta_1 \left( \frac{1}{L_x} (z - \xi_j) \middle| \tau \right) \quad (3.21)$$

where  $\xi_j$  is the position of the  $j$ :th zero. The function  $\vartheta_j$  is defined in equations (A.10) to (A.13) in the Appendix, and has the property that  $\vartheta_1(0|\tau) = 0$ . By demanding that  $\psi(z)$  obeys periodic boundary conditions defined by (3.11) and (3.12), we get relations on  $k$  and  $\xi = \frac{1}{N_s} \sum_j \xi_j$ . Let us restrict  $\xi$  to  $\xi = x_1[m + n\tau] - \frac{L_x}{2}[\tau + 1]$  and define  $z_j = \xi_j + \frac{1}{2}(1 + \tau)L_x$ . The new variable  $z_j$ , is the point on the torus where we expect the maximum, of the coherent state, will be located. This suspicion is based on the geometric consideration, that if all the zeros  $\xi_j$  are at the same point, we will likely find the maximum at the position diametrically opposed to  $\xi$ . In terms of the new variable  $z_j$  the LCS wave function can be brought to the form

$$\psi_{nm}(z) = \mathcal{N}_{nm} e^{-\frac{y^2}{2}} e^{-iy_n z} \vartheta_3 \left( \frac{\pi}{L_x} (z - z_{nm}) \middle| \tau \right)^{N_s}, \quad (3.22)$$

where  $z_{nm} = x_m + x_n \tau$ . All the LCS are generated using  $t_1$  and  $t_2$  such that  $t_1^l t_2^k \psi_{n,m} \propto \psi_{n+k, m+l}$ . Using  $t_2$  and  $t_1$ , the relative normalization of  $\psi_{nm}$  and  $\psi_{n'm'}$  can be deduced, by transforming the different  $\psi_{nm}$  into each other. By inspection we see that  $|\mathcal{N}_{nm}| = \mathcal{N} e^{-\frac{y_n^2}{2}}$ , where  $\mathcal{N} \equiv \mathcal{N}_{00}$ . We will later, in section 3.7, calculate  $\sigma_x \sigma_y$  for  $\psi_{nm}$  and will then use the expression in (3.22) as it is well suited for numerical evaluation. However, for analytic manipulations this is not the most useful way of writing  $\psi_{nm}(z)$ . Furthermore, equation (3.22) also leaves unanswered the question of how to calculate the normalization  $\mathcal{N}_{nm}$ .

To proceed further we need to expand  $\psi_{nm}$  in Fourier modes in such a way that it will resemble (3.18). By hiding parts of the Fourier weight in a constant,  $Z_K$ , we can write  $\psi_{nm}$  as

$$\psi_{nm}(z) = \mathcal{N} \sum_K Z_{K+n} e^{-\frac{1}{2}(y+y_K)^2} e^{iy_K(x-x_m)} e^{i\frac{1}{2}y_K \omega_K} \quad (3.23)$$

where  $Z_K$  is defined as

$$Z_K = \sum_{\substack{\{k_j\}=-\infty \\ \sum_j k_j = K}}^{\infty} e^{i\pi \tau \sum_j \tilde{k}_j^2}. \quad (3.24)$$

The exponential sum runs over  $\tilde{k}_j$ , which is the deviation from the mean value of  $k_j$  such that  $k_j = \frac{K}{N} + \tilde{k}_j$ . This constant  $Z_K$  can, together with a factor  $e^{-i\pi\tau\frac{K^2}{N_s}}$ , for imaginary  $\tau$ , be interpreted as the partition function of  $N_s$  particles on a circle where the total angular momentum is constrained to  $K$ . For our purposes, the most important property is that  $Z_{K+N_s} = Z_K$ . By inspecting (3.22) and (3.23), we can fix the relative normalization as  $\mathcal{N}_{nm} = e^{iy_n(x_m + \frac{1}{2}x_n\tau)}\mathcal{N}$ .

In general, when we wish to calculate the overlap between two wave functions on the torus we might naively think that we would need to choose a region of integration since the torus only spans a domain that is  $\mathbf{L}_1 \times \mathbf{L}_2$ . Because of the periodic boundary conditions, we are guaranteed that any domain  $\mathbf{L}_1 \times \mathbf{L}_2$  will work. Usually what happens is that the  $x$ -integration gives a Kronecker  $\delta$ , that allow us to combine the  $y$ -integral from a piecewise incomplete to a complete integral. The LCS are no exceptions, and with some algebra we find the overlap to be

$$\langle \psi_{n'm'} | \psi_{nm} \rangle = \sqrt{\pi} L_x \mathcal{N}^2 \sum_{l=1}^{N_s} Z_{l+n} \bar{Z}_{l+n'} e^{iy_l(x_{m'} - x_m)}. \quad (3.25)$$

Choosing  $m' = m$  and  $n' = n$  we get

$$\sum_{k=1}^{N_s} |Z_k|^2 = \frac{\mathcal{N}^{-2}}{L_x \sqrt{\pi}} \quad (3.26)$$

that defines the normalization of (3.23). Although numerical values for  $Z_k$  are unknown, we expect that (3.25) will resemble a Gaussian function as  $N_s \rightarrow \infty$ . The argument is most simple for  $m \neq m'$  and  $n = n'$ . If the  $Z_k$  were all constant, then the overlap would reduce to  $\langle \psi_{nm'} | \psi_{nm} \rangle \propto \delta_{mm'}$ . Now, all the terms  $Z_k$  are not equal, but on the same scale. This means that  $\langle \psi_{nm'} | \psi_{nm} \rangle$  has a Gaussian shape centred at  $m = m'$ , that drops to zero as the phases between the different terms will interfere destructively.

We mentioned earlier that the LCS are over-complete, but that this does not pose a problem. The reason for this is that we can form a simple resolution of unity using  $\psi_{nm}$ , which is

$$\mathcal{P}_{\text{LLL}} = \frac{1}{N_s} \sum_{m,n} |\psi_{nm}\rangle \langle \psi_{nm}|. \quad (3.27)$$

A detailed proof of (3.27), and (3.28), is found in Ref [4]. When proving (3.27), it is essential that  $\sum_{m,n} |\psi_{nm}\rangle \langle \psi_{nm}|$  commutes with both  $t_1$  and  $t_2$ , since it implies that it is proportional to  $\mathcal{P}_{\text{LLL}}$ , the projector onto the LLL.

In Section 3.6 we will see that the Continuous Coherent States can form a self-reproducing kernel in the LLL. This means that the coherent states work just like a  $\delta$ -function, giving  $\int d^2w \varphi_w(z) \psi(w) = \psi(z)$ , when  $\psi(z)$  is a LLL wave function. For the LCS, there exists a similar kernel and it can be formulated as

$$\phi(z) = S^{-1} \sum_{m,n=1}^{N_s} e^{i\frac{1}{2}y_n\omega_n} \psi_{mn}(z) \phi(z_{mn}) \quad (3.28)$$

where  $\psi(z)$  again is an arbitrary wave function in the LLL and  $z_{mn} = x_m + x_n\tau$ . Equation (3.28) is established by first proving the equation on a sub-lattice  $z = z_{lp}$ , and then arguing that these are enough points for the formula to be valid for all  $z$  in the fundamental domain. We can view (3.28) as a map  $\mathcal{P}_{\text{LCS}}$ , from the space of arbitrary wave functions  $\phi(z, z^*)$  to the LLL wave functions.

In establishing equation (3.28) we have showed that  $\mathcal{P}_{\text{LCS}}\psi = \mathcal{P}_{\text{LLL}}\psi$ , if  $\psi$  is in the LLL. We should however be aware that (3.28) does *not* represent a true projection operator  $\mathcal{P}_{\text{LLL}}$ .

The reason is that (3.28) on components that are not in the LLL, does in general not vanish. This is seen by considering  $\delta(z - z')$ , which has components in all Landau levels, especially in the LLL. It is obvious that  $\mathcal{P}_{\text{LCS}}\delta(z - z')$  will be zero, even though we know that  $\delta(z - z')$  has components in the LLL. Thus the effect of  $\mathcal{P}_{\text{LCS}}$  is that the contributions from non-LLL states precisely cancel the LLL part, except at  $z' = z_{mn}$  for which the contribution is divergent. This statement can be made somewhat sharper by considering the simplest case of  $N_s = 1$  – where each Landau level has only one state,  $\eta_n$ . By a simple parity argument, we can show that  $\mathcal{P}_{\text{LCS}}\eta_{2n+1} = 0$  whereas  $\mathcal{P}_{\text{LCS}}\eta_{2n} \neq 0$ . We suspect that the result for  $N_s = 1$  is valid for arbitrary  $N_s$ , meaning that  $\mathcal{P}_{\text{LCS}}\psi = \mathcal{P}_{\text{LLL}}\psi$ , if  $\psi$  is in an odd numbered LL (or the LLL), but are otherwise different.

### 3.6 Continuous Coherent states (CCS)

In the previous Section we introduced the LCS wave functions as a candidate for coherent states. One of the problems with the LCS is that they are only defined on a lattice  $z_{nm}$  and not for generic points on the torus. We would like to have a recipe for constructing localized wave functions around some other points than the ones allowed for by the LCS. A natural way of constructing these states would be to project a  $\delta$ -function on the LLL. These functions will automatically fulfil the correct boundary conditions and will hopefully be localized at the base of the  $\delta$ -function. We thus define the state

$$\varphi_w(z) = \mathcal{P}_{\text{LLL}}\delta^{(2)}(z - w) \quad (3.29)$$

where  $w = x' + iy'$  as our Continuous Coherent States (CCS). The projector  $\mathcal{P}_{\text{LLL}}$  can either be expressed in terms of basis states  $\mathcal{P}_{\text{LLL}} = \sum_s |\eta_s\rangle \langle \eta_s|$  or in terms of LCS as  $\mathcal{P}_{\text{LLL}} = \frac{1}{N_s} \sum_{mn} |\psi_{nm}\rangle \langle \psi_{nm}|$ . Since  $\mathcal{P}_{\text{LLL}}^2 = \mathcal{P}_{\text{LLL}}$ , we directly have that  $\langle \varphi_{w'} | \varphi_w \rangle = \varphi_w(w')$  which shows that these states are in general not normalized. From the definition of  $\varphi_w(z)$  also follows a resolution of unity

$$\psi(z) = \int d^2w \varphi_w(z) \psi(w)$$

for states in the LLL and zero otherwise. Whatever form of  $\mathcal{P}_{\text{LLL}}$  we choose, we will get the expression

$$\begin{aligned} \varphi_w(z) = & \frac{1}{L_x \sqrt{\pi}} \sum_{K,t} e^{-\frac{1}{2}(y+y_K)^2} e^{-\frac{1}{2}(y'+y_K+L_y t)^2} \times \\ & \times e^{-iy_K(x'-x)} e^{-i(\omega_K+x')L_y t} e^{-i\frac{1}{2}L_y L_\Delta t^2}. \end{aligned} \quad (3.30)$$

We need to rewrite this expression in terms of  $\vartheta$ -functions as these naturally incorporate the boundary conditions on the torus. We first identify the sum over  $K$  with a  $\vartheta$ -function. We get the still quite complicated expression

$$\varphi_w(z) = \frac{e^{-\frac{1}{2}(y^2+y'^2)}}{L_x \sqrt{\pi}} \sum_t e^{i2\pi t \frac{N_s}{2} T^+} e^{i\pi i \Im(\tau) \frac{N_s}{2} t^2} \vartheta \left[ \frac{-t \frac{N_s}{2}}{t \Re(\tau)} \right] \left( T^- \middle| \frac{2}{N_s} i \Im(\tau) \right)$$

where  $T^\pm$  is defined as  $T^\pm = \frac{1}{L_x} (z \pm \bar{w})$ .

Let us first study the special case of  $\Re(\tau) = 0$ , such that we assume that  $\tau$  is purely imaginary as  $\tau = i \frac{L_y}{L_x}$ . Even and an odd number of fluxes  $N_s$ , will have  $\varphi_w$  with slightly different functional

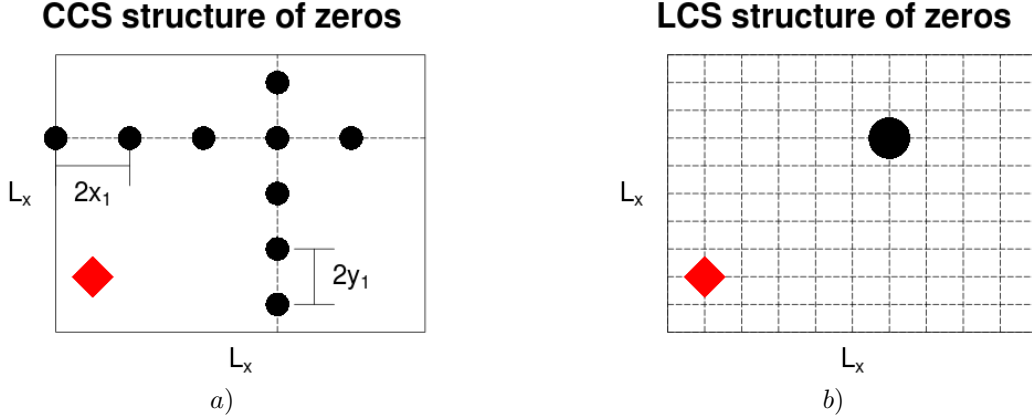


Figure 3.2: Structure of zeros and maxima for a) Continuous Coherent States  $\varphi_w$  and b) Lattice Coherent States  $\psi_{mn}$ . In both pictures, the red diamond ( $\blacklozenge$ ) is centred at the maximum. The black circles ( $\bullet$ ) represent the locations of the zeroes. The larger black circle indicates that the zero is  $N_s$ -fold. On the rectangular ( $\Re(\tau) = 0$ ) torus, for  $N_s$  being an even number, the zeros of the CCS form a “cross” centred over  $z = w$ .

forms. In the even case,  $t \frac{N_s}{2}$  is an integer and we may ignore it in the argument of  $\vartheta$  and directly identify the sum over  $t$  as another  $\vartheta$ -function such that

$$\varphi_w(z) = \frac{e^{-\frac{1}{2}(y^2 + y'^2)}}{L_x \sqrt{\pi}} \vartheta_3\left(\frac{N_s}{2} T^+ \middle| \frac{N_s \tau}{2}\right) \vartheta_3\left(T^- \middle| \frac{2\tau}{N_s}\right). \quad (3.31)$$

In contrast, if  $N_s$  is odd, we have to split the sum over  $t$  into even and odd terms. We can then identify the even and odd sums over  $t$  separately as  $\vartheta$ -functions. The resulting wave function is

$$\varphi_w(z) = \frac{e^{-\frac{1}{2}(y^2 + y'^2)}}{L_x \sqrt{\pi}} \sum_{j=2,3} \vartheta_j(T^+ N_s | 2N_s \tau) \vartheta_j\left(T^- \middle| \frac{2\tau}{N_s}\right). \quad (3.32)$$

Different functional forms are obtained depending on whether  $N_s$  is even or odd. This is related to the structure of the zeros. For an even number of zeros, they will divide into two groups that translate rigidly under guiding centre translations. For an odd number of zeros, these rigid translations do not occur. The reason is because there now exists an extra zero that constrains the movements of the other zeros.

For generic values of  $\Re(\tau)$  we can make some progress by assuming that  $\Re(\tau)$  is a rational number  $\Re(\tau) = \frac{p}{q}$ . For simplicity, we consider only an even number of fluxes. The sum over  $t$  can then be split into smaller pieces  $t = k + q \cdot n$  such that  $\sum_{t=-\infty}^{\infty} = \sum_{k=1}^q \sum_{n=-\infty}^{\infty}$ . These different sums can separately be identified as  $\vartheta$ -functions such that

$$\varphi_w(z) = \frac{e^{-\frac{1}{2}(y^2 + y'^2)}}{L_x \sqrt{\pi}} \sum_{k=1}^q \vartheta\left[\begin{matrix} \frac{k}{q} \\ 0 \end{matrix}\right] \left(\frac{q N_s}{2} T^+ \middle| \frac{N_s}{2} q^2 i \Im(\tau)\right) \vartheta\left[\begin{matrix} 0 \\ k \frac{p}{q} \end{matrix}\right] \left(T^- \middle| \frac{2}{N_s} i \Im(\tau)\right).$$

For the coherent states with an odd number of fluxes, the situation is somewhat more complicated, but the logic is the same as for even fluxes. The precise division of  $t$  will now depend on whether  $q$  is an even or odd number.



Since we know where the zeros of the function  $\vartheta_3$  are located – see equation (A.2) – we can deduce the location of the zeros for  $\varphi_w$  in the case of  $\Re(\tau) = 0$  and  $N_s$  being even. The zeros of  $\varphi_w$  are at  $z = x_{2m+1} - x' + \imath(y' + (\frac{1}{2} + n)L_y)$  and  $z = \imath(y_{2n+1} - y') + x' + (\frac{1}{2} + m)L_x$ . The zeros lie on two perpendicular axes intersecting at  $z = w + \frac{1}{2}(L_x + \imath L_y)$ , as depicted in Figure 3.2a. We conclude that as  $\tau$  is transformed away from purely imaginary, the nice linear pattern formed by the zeros is broken.

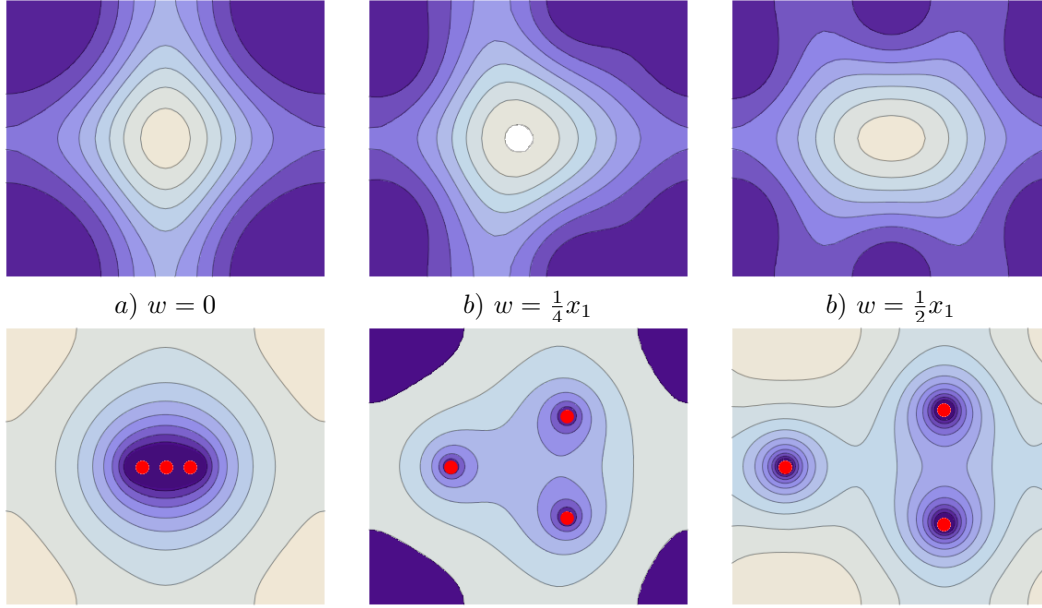


Figure 3.3: *Upper panel* : The spatial profile of CCS at  $N_s = 3$  for  $\tau = \sqrt{\frac{3}{4}}\imath$  where a)  $w = 0$ ; b)  $w = \frac{1}{4}x_1$ ; and c)  $w = \frac{1}{2}x_1$ . These correspond to a rectangular lattice where  $w$  is moved away from  $w = 0$ . The fundamental domain is centred around  $r = w$ . Notice how the spatial profile changes as  $w$  is tuned away from  $w = 0$ . The reason is that the zeros of  $\varphi_w$  move around. *Lower panel*: Positions of the zeros are represented by filled red circles ( $\bullet$ ), for the same values of  $w$  as in the upper panel. Here the domain is fixed with a centre at  $r = \frac{1}{2}(1 + \tau)x_1$  to facilitate the tracking of zeros.

Further, as we change  $w \rightarrow w + \delta w$  half of the zeros will be propagating in the direction of  $\delta w$  while the other half of the zeros will move in the direction of  $-\delta w$ . This behaviour ensures that the boundary conditions are always respected. The location of the zeroes in  $\varphi_w$  are  $w$  dependent, and as a consequence the spacial distribution of  $\varphi_w$  also depends on  $w$ . This is illustrated in the upper panel of Figure 3.3, for an odd number of particles. Here we plot in the upper panel, the contours of  $|\varphi_w|^2$  for  $N_s = 3$  and  $\tau = \sqrt{\frac{3}{4}}\imath$ . The constraint from boundary conditions on the locations of the zeros is nicely illustrated in the lower panel of Figure 3.3. In the lower panel, we plot  $\log|\varphi_w|$  and highlight the zeros of  $\varphi_w$  with a filled red circle ( $\bullet$ ). The columns in the Figure are organized such that a) has  $w = 0$ , b) has  $w = \frac{1}{4}x_1$  and c) has  $w = \frac{1}{2}x_1$ . For the upper panel, the fundamental domain is centred at  $z = w$  and in the lower panel the centre of the fundamental domain is at  $z = \imath\frac{1}{2}(1 + \tau)L_x$ .

As the probability distribution of  $\varphi_w$  depends on  $w$ , the delocalization  $\sigma_x\sigma_y$  must also depend on  $w$ . In Figure 3.4, we can see how  $\sigma_x\sigma_y$  varies as a function of  $w$ . In the corners, where

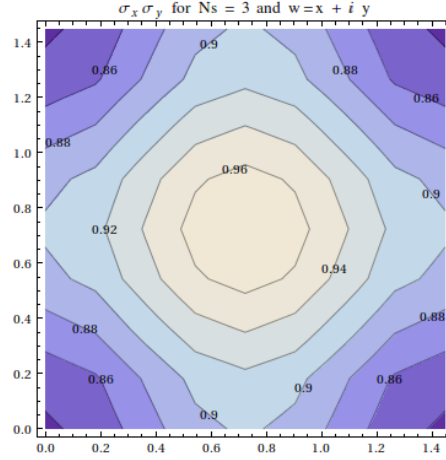


Figure 3.4: The spatial delocalization of  $\varphi_w$  is measured as  $\sigma_x \sigma_y$  for  $\tau = i$  with variation of  $w$ . Darker colour corresponds to lesser delocalization. The delocalization of  $\varphi_w$  depends on  $w$ .

$w = x_n + \tau x_m$  the delocalization is at a minimum. In the centre, where  $w = x_{n+\frac{1}{2}} + \tau x_{m+\frac{1}{2}}$ , the delocalization is at a maximum.

### 3.7 Localization behaviour of LCS and CCS

The previous sections have analysed the LCS and the CCS, that are candidates for localized wave functions. This chapter will take the analysis one step further and quantify the spatial delocalization  $\sigma_x \sigma_y$  for these states. As we have alluded to earlier, we can not make an analogous calculation to the ones performed in sections 3.1 and 3.2, where we used the ladder operators for an algebraic calculation. It is however possible to numerically evaluate the  $\sigma_x \sigma_y$  delocalization using

$$\langle A(x, y) \rangle_\Omega = \int \int_\Omega dx dy A(x, y) |f(x, y)|^2 \quad (3.33)$$

where  $A(x, y)$  is some operator and  $f(x, y)$  can be either  $\varphi_w(z)$  or  $\psi_{nm}(z)$ . The uncertainty in variable  $A$  is defined as  $\sigma_A^2 = \langle A^2 \rangle - \langle A \rangle^2$ .

Since the mean value is not well defined on a periodic structure, we need to be careful when we choose the region  $\Omega$  in which we evaluate the integral (3.33). A natural choice of the centre  $(x_0, y_0)$  of  $\Omega$ , is such that  $\langle x \rangle_{x_0, y_0} = x_0$  and  $\langle y \rangle_{x_0, y_0} = y_0$ . Here we need to be careful as there always exists more than one point in any periodic domain that fulfils  $\langle x \rangle_{x_0, y_0} = x_0$  and  $\langle y \rangle_{x_0, y_0} = y_0$ . To be thorough, we should choose the point  $(x_0, y_0)$  where  $\langle x^2 \rangle_{x_0, y_0}$  and  $\langle y^2 \rangle_{x_0, y_0}$  are minimal.

Figure 3.5 shows how the delocalization depends on the number of fluxes,  $N_s$ . We will examine the high,  $N_s \rightarrow \infty$ , and the low,  $N_s \rightarrow 0$ , flux limits.

#### 3.7.1 The low flux limit $N_s = 1, 2, 3, 4$ .

In Figure 3.5, we first consider the low values of  $N_s$ , such as  $N_s = 2, 3, 4$ . We see that  $\sigma_x \sigma_y < 1$ , which naively is contradictory to the limit  $\sigma_x \sigma_y \geq 1$  set by the Heisenberg uncertainty relation. This issue is resolved when considering the finite geometry of the torus. This finite geometry

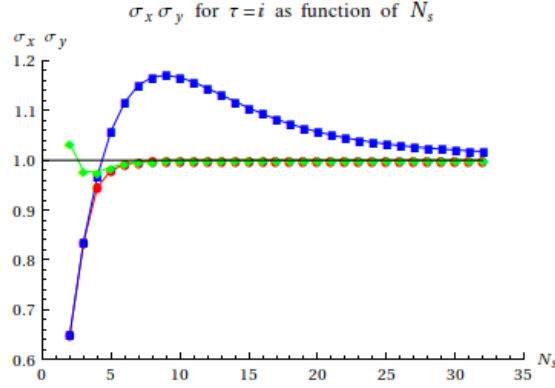


Figure 3.5: The spatial delocalization of  $\varphi_w$  and  $\psi_{nm}$  measured as  $\sigma_x \sigma_y$  for  $\tau = i$  and different  $N_s$ . The colour code is: (Red) for  $\varphi_w$  with  $w = x_m + \tau x_n$ ; (Green) for  $\varphi_w$  with  $w = x_m + \frac{1}{2} + \tau x_n + \frac{1}{2}$ ; and (Blue) for  $\psi_{nm}$ . The CCS in general displays smaller delocalization than the LCS but the delocalization of CCS depends on  $w$ . The LCS and minimal CCS delocalization are the same for  $N_s = 1, 2, 3$  for  $\tau = i$  since their zeros coincide at these fluxes. We have excluded the point a  $N_s = 1$  since only one state exists at that flux.

gives an upper bound to how large any delocalization can be. The maximum delocalization, that of a uniform distribution, has  $\sigma_x = \frac{1}{\sqrt{3}} \frac{L}{2}$ , where  $L$  is the linear width. The main point is that, if the imaginary part of  $\tau$  is far from 1, we can have  $L_x \ll 1$  and  $L_y \gg 1$  such that  $\sigma_y \approx 1$  and  $\sigma_x \propto L_x$ . An illustrative example of this is the basis states  $\eta_s$ , that have  $\sigma_x \approx \frac{1}{\sqrt{3}} \frac{L_x}{2}$  and  $\sigma_y \approx \frac{\sqrt{\pi}}{2}$  such that  $\sigma_x \sigma_y \approx \frac{\pi}{2\sqrt{6}} \sqrt{\frac{N_s}{\Im(\tau)}}$ , if  $\Im(\tau) \gtrsim 1$ . It is obvious that even these states will, for  $\Im(\tau)$  large enough, violate the uncertainty relation formulated on the plane. Therefore, it is only to be expected that the coherent states may violate the uncertainty relation as well. We can now explain why  $\sigma_x \sigma_y < 1$  for the low values of  $N_s$  in Figure 3.5. The coherent state simply extends over the entire torus such that the bounds on  $\sigma_x \sigma_y$  do not originate from  $\varphi_w$ , but rather from the small toroidal size.

### 3.7.2 The Thermodynamic limit $N_s \rightarrow \infty$ .

We now inspect Figure 3.5 again. This time we are interested in the delocalization, as the number of fluxes increase. We can see that as  $N_s \rightarrow \infty$  both the LCS and CCS approach  $\sigma_x \sigma_y = 1$ , which is the result on the plane. It is noteworthy that the CCS converge really fast: At  $N_s > 10$  the CCS have already saturated at the delocalization expected on the plane, whereas it takes  $N_s > 40$  for the LCS to reach the same delocalization. For small values of  $N_s$ , the delocalization for  $w \neq 0$  can actually be higher than the delocalization of the corresponding LCS. However already at  $N_s = 9$ , the maximum and minimum of the delocalization are practically indistinguishable for the CCS.

### 3.7.3 Changing the Aspect Ratio of the Torus

As we change the aspect ratio of the torus, and let  $\Im(\tau) \rightarrow \infty$ , a similar thing should happen as for low flux. The magnetic length  $\ell = 1$ , is larger than the linear length of the torus  $1 > L_x$ . As a consequence we expect  $\sigma_x \sigma_y \geq 1$  to be violated. The expected behaviour of  $\sigma_x \sigma_y$  as  $\Im(\tau) \rightarrow \infty$ ,

is clearly visible in Figure 3.6a. There we see that as  $\Im(\tau) \rightarrow \infty$  then  $\sigma_x \sigma_y \propto \frac{1}{\sqrt{\Im(\tau)}}$ . We also see that there is a wide region of  $\tau$  where the CCS has lower  $\sigma_x \sigma_y$  than the LCS.

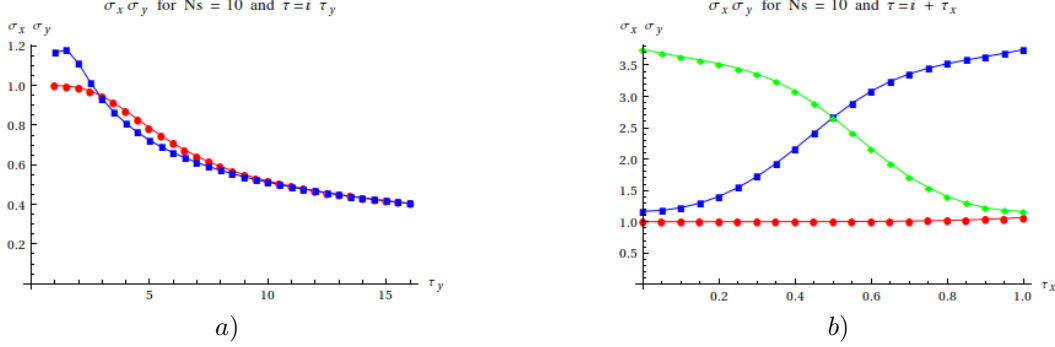


Figure 3.6: The delocalization of CCS (Red) and LCS (Blue) at  $N_s = 10$  as  $\tau$  is varied. a)  $\tau = i\tau_y$  where  $\tau_y$  is varied. The CCS have better delocalization than the LCS over a region in  $\tau$ -space around  $\tau = i$ . b)  $\tau = i + \tau_x$ , where  $\tau_x$  is varied. The third line (Green) shows  $\sigma_x \sigma_y$  calculated for LCS but with  $\Omega$  defined by the corners  $0, L_x, \tau L_x$  and  $\tau L_x - L_x$  instead of  $0, L_x, \tau L_x$  and  $\tau L_x + L_x$ . This line is included to show that at  $\tau \rightarrow \tau + 1$  we get localized states again, but in a different region.

### 3.7.4 Changing the Skewness of the Torus

Figure 3.6b shows what happens if we change the real part of  $\tau$  and keep the imaginary part fixed at  $\Im(\tau) = 1$ . It is clear that the CCS wave functions stay localized whereas the LCS delocalization grows with  $\Re(\tau)$ . It is indeed interesting what goes on here. We can see that since  $\sigma_x \sigma_y$  increases with  $\Re(\tau)$ , the state  $\psi_{nm}$  is no longer properly localized with respect to the fundamental region centred at  $z = w$ . Comparing  $\psi_{nm}$  for  $\tau = i$  and  $\tau = i + 1$ , it looks as if the maxima have been shifted by half a period. Instead of being at  $z = z_{nm}$  the maxima of  $\psi_{nm}$  is at  $z = z_{nm} + \frac{L_x}{2}$ . Mathematically this happens since  $\vartheta_3\left(\frac{\pi}{L_x}z \middle| \tau + 1\right) = \vartheta_3\left(\frac{\pi}{L_x}\left(z - \frac{L_x}{2}\right) \middle| \tau\right)$ , which explains why  $\sigma_x \sigma_y \propto \sqrt{N_s}$  at  $\tau = 1 + i$ . Even more noteworthy, the path the maxima takes as  $\tau \rightarrow \tau + 1$  is non-trivial. Clearly the maximum is no longer in the centre of the domain  $L_x \times \tau L_x$  but rather at the centre of the domain  $L_x \times (\tau + 1)L_x$ . Indeed the maximum splits up into two separate maxima. This effect is depicted in the lower panel of Figure 3.7 where we see how the spatial profile of  $\psi_{nm}$  changes as  $\tau$  is tuned away from  $\Re(\tau) = 0$ . As  $\tau$  approaches  $\Re(\tau) = 1$ , each maximum will recombine with another maximum to finally get the single maximum localized at  $z = z_{nm} + \frac{L_x}{2}$  at  $\tau = \tau + i$ .

We believe that we must always have this splitting of the maximum into two maxima at  $\tau = i\tau_y \rightarrow \tau = i\tau_y + \frac{1}{2}$  regardless of the value of  $\tau_y$ . The argument goes as follows and is illustrated in Figure 3.8: For  $\tau = i\tau_y$ , the fundamental domain is a square and the point that is the furthest from all zeros is located at the centre of the domain, assuming the zeros are at the edges. By symmetry we argue that the maxima is at this point. At  $\tau = i\tau_x + \frac{1}{2}$ , the geometry of the fundamental domain has changed to that of two joined triangles and there no longer exists a unique point that is farthest from all zeros. We can therefore not directly determine the position of the maximum. Instead there exists two possibilities for the maximum, and both of them will induce multiple maxima. The *first* alternative is the point at the centre of the fundamental domain,  $z = \frac{1}{2}(1 + \tau)L_x$ , shown with a star ( $\star$ ) in Figure 3.8b. However at this

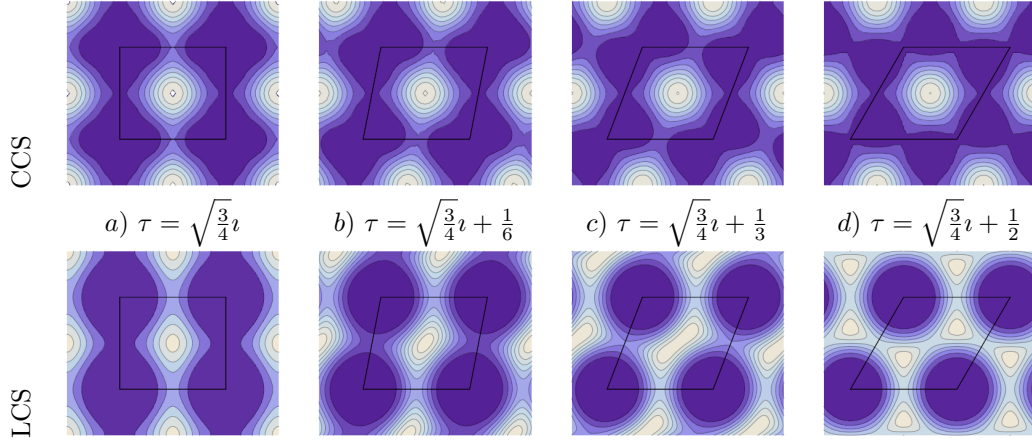


Figure 3.7: The spatial profile of CCS (*Upper panel*) and LCS (*Lower panel*) at  $N_s = 4$  for  $\tau = \sqrt{\frac{3}{4}}\iota + \tau_x$  where  $\tau_x = 0, \frac{1}{6}, \frac{1}{3}, \frac{1}{2}$ . The given  $\tau_x$  correspond to a rectangular, two general and one triangular lattice. The black contours show the fundamental domain. The CCS nicely reshape itself whereas the LCS become massively distorted. Here lighter colour corresponds to larger values of  $|\psi|^2$ .

geometry, because of symmetry, an equivalent point exists also at  $z = \frac{1}{2}\tau L_x$ , also shown with a star. Because of symmetry, any maximum that is at any of these points must also be at the other, leading to at least a twofold splitting of the maxima.

The *second* alternative is to place the maximum somewhere in one of the triangles, such as in  $z_{\max} = \frac{1}{2}L_x + iqL_y$  where  $0 < q < 1$  depending on  $\tau_y$ . Due to symmetry there exists an equivalent point at  $z = (1 + \tau)L_x - z_{\max}$ . The two points are marked with a plus (+) in the figure. Both the alternatives for the location of the maximum results in at least a twofold maxima. We believe in the latter alternative: Apart from the suggestive lower panel of Figure 3.7, the reason is that at the special case of  $\tau = \sqrt{\frac{3}{4}}\iota + \frac{1}{2}$ , we effectively have a triangular lattice and the maximum at ( $\star$ ) would be threefold split.

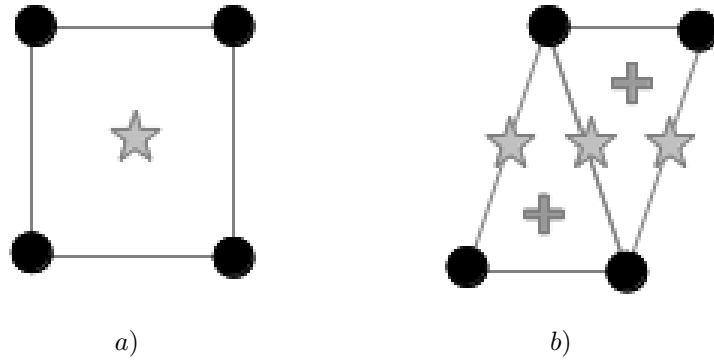


Figure 3.8: The analysis for how the zeros and maxima of the of the LCS are located. *a)* In the square case  $\Re(\tau) = 0$  there is a unique point farthest from all zeros. This unique point is marked with a star ( $\star$ ). *b)* For the triangular case  $\Re(\tau) = \frac{1}{2}$  where are two alternatives marked with stars ( $\star$ ) and pluses (+). We believe that the maxima will always be at the pluses.

The conclusion we should draw is that at and around  $\tau = \nu\tau_y + \frac{1}{2}$ , the LCS has a twofold split maximum and can therefore not be localized. There is reason to believe that the region around  $\tau = \nu\tau_y + \frac{1}{2}$ , that supports double maxima, will be non-vanishing even in the thermodynamic limit  $N_s \rightarrow \infty$ . This is since the symmetries described above still exist and the maxima will be sufficiently separated that small variations in  $\tau$  should not affect the stability of the individual maximum.

It might feel uncomfortable that we violate the Heisenberg uncertainty relation (3.1), when we calculate  $\sigma_x\sigma_y$  on the torus. We should remember, that we violate (3.1) because neither  $x$  nor  $y$  are well defined operators on the torus. By well defined, we mean that  $\langle\psi|\mathcal{O}|\phi\rangle$  should not depend on the position of the torus fundamental domain  $\Omega$ . Given that  $\sigma_x\sigma_y$  is not well defined on the torus, it is reasonable to question the above analysis all together. We are however still interested in  $\sigma_x\sigma_y$  for two reasons. First,  $\sigma_x\sigma_y$  is still a measure of the delocalization of a particle, provided  $\Omega$  is chosen properly. Second, in the thermodynamic limit  $N_s \rightarrow \infty$ , the area of the torus diverges and we approach the planar limit. In this limit both  $x$  and  $y$  recover well defined definitions.

## Chapter 4

# Trial Wave Functions from Conformal Field Theory

So how do the coherent states on the torus relate to conformal field theory? The connection between the FQHE and CFT lies in the description of the quasi-particles. It can be shown that the topological information in a FQH-state can be described using an effective Chern-Simons theory. The same theory is also conjectured to describe the edge excitations of the same FQH-state[31]. It is further conjectured that trial wave functions with correct topological properties may be extracted from correlation functions of CFTs with suitable operators[20].

The Laughlin wave function at filling fraction  $\nu = \frac{1}{q}$  will serve as an introductory example. Simply put, the norm of the wave function  $|\psi_{\text{Laughlin}}|^2$  can be obtained as a correlation function of a CFT, with primary fields and a suitable background charge, such that

$$|\psi_{\text{Laughlin}}|^2 \propto \left\langle \mathcal{O}_{\text{bg}} \prod_{i=1}^{N_e} V(\mathbf{r}_i) \right\rangle \propto \prod_{i<j}^{N_e} |z_i - z_j|^{2q} \exp \left\{ - \sum_{i=1}^{N_e} \frac{1}{2} |z_i|^2 \right\}.$$

Here  $V(\mathbf{r})$  is a vertex-operator that represents an electron at position  $\mathbf{r}$ . The background operator  $\mathcal{O}_{\text{bg}}$  is needed in order to make the whole correlator charge neutral, as well as to represent the charged atomic background. We now add, that a many-particle wave function in the LLL can always be written as  $\psi_{\text{LLL}} = \exp \left\{ - \sum_{i=1}^{N_e} \frac{1}{4} |z_i|^2 \right\} \cdot f(\{z_i\})$ , where  $f(\{z_i\})$  is a holomorphic function. This enables us to factorize the correlation function into a holomorphic, an anti-holomorphic, and a Gaussian part as

$$\begin{aligned} \left\langle \mathcal{O}_{\text{bg}} \prod_{i=1}^{N_e} V_i(\mathbf{r}_i) \right\rangle &\propto \left( \prod_{i<j}^{N_e} (z_i - z_j)^q \cdot \exp \left\{ - \sum_{i=1}^{N_e} \frac{1}{4} |z_i|^2 \right\} \right) \times \\ &\times \left( \prod_{i<j}^{N_e} (\bar{z}_i - \bar{z}_j)^q \cdot \exp \left\{ - \sum_{i=1}^{N_e} \frac{1}{4} |z_i|^2 \right\} \right). \end{aligned}$$

Thus, by taking the square root of the correlation function we can reconstruct the Laughlin wave function (2.1). The factorization of the correlator is more than symbolic. On the plane and sphere, the vertex operator  $V(\mathbf{r})$  can be split into a holomorphic  $V(z)$  and an anti-holomorphic part  $\bar{V}(\bar{z})$ , that can be evaluated independently. On the torus, the separation into holomorphic

and anti-holomorphic is not as clean, as there exists zero-modes, due to the possibility of winding around the torus handles.

For other states, higher up in the hierarchy the method is the same, *i.e.* we construct the trial wave function as a correlator of electron operators. The main difference is that not all electrons are equivalent. Some electrons will reside in higher LLs, giving rise to  $\bar{z}$  components in the wave function. Under projection to the LLL these components are transformed into holomorphic derivatives  $\partial_z$ , acting on the remaining wave function[6].

In fact, any state within the hierarchy that can be formed through condensation of quasi-particles, can be expressed in a similar way as  $\psi_{\text{Laughlin}}$ , but with some added complexity. First, there is usually more than one type of electron operator  $V^{(\alpha)}$ . Second, there are external derivatives  $\partial_z$  acting on the correlator. Third, the whole wave functions needs to be antisymmetrized explicitly, since all electrons are not treated on equal footing. Taking all of the above considerations into account, the square of the Hierarchy wave function may be written symbolically as

$$|\psi_{\text{Hierarchy}}|^2 \propto \mathcal{A} \left\{ [\text{Derivatives}] \left\langle \mathcal{O}_{\text{bg}} \prod_{\alpha} \prod_{i_{\alpha} \in I_{\alpha}} \hat{V}^{(\alpha)}(\mathbf{r}_{i_{\alpha}}) \right\rangle \right\}. \quad (4.1)$$

In the above equation,  $\mathcal{A}$  denotes antisymmetrization over electrons, and  $\prod_{\alpha}$  partitions the electrons into different inequivalent sets. The derivatives come about because some of the electron operators  $V^{(\alpha)}(z)$  are describing the hierarchical fusing of quasi-particles and electrons. This manifests itself through the appearance of derivatives in the vertex operators  $V^{(\alpha)}(z) = \partial_z^{\alpha-1} \hat{V}^{(\alpha)}(z)$ .

On the torus, we usually use a different gauge, such that

$$\psi_{\text{LLL}} = \exp \left\{ - \sum_{i=1}^{N_e} \frac{1}{2} y_i^2 \right\} \cdot f(\{z_i\}).$$

Also, we expect a ground state degeneracy that can be divided by the denominator  $q$ , of the filling fraction  $\nu = \frac{p}{q}$ [8]. For the simplest abelian FQH states the degeneracy is exactly  $q$ . The ground state degeneracy makes the analysis of the CFT construction more involved but the basic idea is the same. We are still using electron operators  $V_i^{(\alpha)}(\mathbf{r}_i)$ , such that the correlator is calculated using (4.1). The problem arises here after we have constructed the correlator for the many-particle wave function, and need to act with the external derivatives. These derivatives do not respect the boundary conditions for the single particle states, and we are interested in how to modify these on the torus. We thus seek operators that preserve the boundary conditions, and give us a  $q$ -fold set of trial wave functions. A natural candidate is  $\mathcal{P}_{\text{LLL}} \partial_x$ , the derivative projected to the LLL. In the coming chapter this projection will give some insight to what operator should be used on the torus. We find that after projection the derivative turns into a linear combination of translation operators as

$$\mathcal{P}_{\text{LLL}} \partial_z = \sum_l a_l t_1^l \equiv \mathcal{D}.$$

For a many-particle state a product of derivatives would be

$$\mathcal{P}_{\text{LLL}} \prod_i \partial_{z_i} = \prod_i \mathcal{D}_i.$$

We can however show that  $\prod_i \mathcal{D}_i$  does *not* commute with  $T_2^k = \prod_j t_{2,j}^k$  for any value of the power  $k$ . This means that  $\prod_i \mathcal{D}_i$  changes the quantum numbers in such a way that the  $q$ -fold



degeneracy is lost. The only terms in  $\prod_i \mathcal{D}_i$  that do not change the  $q$ -fold degenerate subspace of the wave functions, are on the form  $T_1^k = \prod_i t_{1,i}^k$ . These are the terms that were used in Ref. [12] when they first addressed this problem.

A related problem is connected with the description of hole-condensates, briefly mentioned in Section 2.3, where terms that include powers of  $\bar{z}$  are generated. These anti-holomorphic terms cause the wave function to be located in higher Landau levels, such that it has to be projected down to the lowest one. In symmetric gauge, this is readily done by the substitution  $\bar{z} \rightarrow \partial_z$ . On the torus, in Landau gauge, the prescription  $\bar{z} \rightarrow \partial_z$  will not work, and it is not clear what should replace it. The idea in this thesis is to use coherent states as a way to project the wave functions to the LLL, by interpreting the correlators as coefficients for the coherent state wave functions[29, 28]. We will in the following sections treat the anti-holomorphic  $\bar{z}$  components, and the external derivatives  $\partial_z$ , in order.

## 4.1 A Concrete Example: The Modified Laughlin State

Let us take a concrete example of how the coherent state kernel can be used to project onto the LLL. We here consider states that contains both  $z$  and  $\bar{z}$  components, but no derivatives. An example of such a state, is a modification of the Laughlin state at  $\nu = \frac{1}{q}$ , first proposed by Girvin and Jach[6] on the plane. They proposed a short distance modification

$$e^{-\frac{q+2p}{4q} \sum_j |z_j|^2} \prod_{i < j} (\bar{z}_i - \bar{z}_j)^p (z_i - z_j)^{q+p},$$

to the Laughlin wave function (2.1). After convolution with the coherent state kernel, the LLL projection was cast in the form

$$e^{-\frac{1}{4} \sum_j |z_j|^2} \prod_{i < j} (\partial_{z_i} - \partial_{z_j})^p (z_i - z_j)^{q+p}, \quad (4.2)$$

where the  $\bar{z}_i$  terms were replaced by derivatives  $\partial_{z_i}$ [6]. This state can be obtained using CFT correlators, either on the plane or the torus, as a representation in the space of coherent states. The wave function obtained from the CFT correlator  $\psi(z, \bar{z})$ , will in general contain both holomorphic coordinates  $z$ , as well anti-holomorphic coordinates  $\bar{z}$ . This wave functions should not be interpreted directly in the the electron coordinate basis  $(z, \bar{z})$ , but rather in the over complete basis of coherent states  $\varphi_\xi$ . Interpreting  $\psi(z, \bar{z})$  as the weight for the CS state  $\varphi_\xi(z)$ , is the same as projecting onto the LLL, such that

$$\mathcal{P}_{\text{LLL}} \psi(z, \bar{z}) = \int d^2 \xi \, \psi(\xi) \cdot \varphi_\xi(z). \quad (4.3)$$

As a direct consequence of (4.3), it can be proven that the boundary conditions that hold for  $\psi(\xi)$ , will also hold for  $\mathcal{P}_{\text{LLL}} \psi(z, \bar{z})$ . The relation before and after projection is trivial, because the magnetic translation operators commutes with  $\mathcal{P}_{\text{LLL}}$ . This fact is easily realized since  $\mathcal{P}_{\text{LLL}} = \prod_{n=1} \left(1 - \frac{a^\dagger a}{n}\right)$  contains only the operator  $a$ , and  $t(\alpha) = e^{\alpha b^\dagger - \bar{\alpha} b}$  contains only the operator  $b$ . These two operators,  $\mathcal{P}_{\text{LLL}}$  and  $t(\alpha)$ , therefore commute, by the definition of  $a$  and  $b$ . Thus, assuming periodic boundary conditions, such as  $t(\mathbf{L}_k) \psi(\xi) = e^{i\phi_k} \psi(\xi)$ , then the same conditions apply for  $t(\mathbf{L}_k) \mathcal{P}_{\text{LLL}} \psi(z, \bar{z}) = e^{i\phi_k} \mathcal{P}_{\text{LLL}} \psi(z, \bar{z})$ .

We will now use the basis of coherent states, to find a torus version of (4.2), with well defined boundary conditions. For the full procedure of constructing wave functions on the torus,

see Ref. [12]. What is important is that we have the same kind of short distance behaviour on the torus, as on the plane. We must also obtain the same  $q$ -fold degeneracy as for the ordinary torus Laughlin state. All states with the short distance behaviour  $z_{ij}^{q+p} \bar{z}_{ij}^p$  can be calculated in the same formalism. Hence we will deal with them simultaneously. On the torus, the polynomial Jastrow factor  $\prod_{i<j} (z_i - z_j)^{q+p} (\bar{z}_i - \bar{z}_j)^p$  must be replaced by Jacobi  $\vartheta$ -functions as

$$\prod_{i<j} \vartheta_1 \left( \frac{1}{L_x} (z_i - z_j) \middle| \tau \right)^{p+q} \vartheta_1 \left( -\frac{1}{L_x} (\bar{z}_i - \bar{z}_j) \middle| -\bar{\tau} \right)^p.$$

The Gaussian factor must be present, and there will also be a centre of mass component, that is absent on the plane. All these pieces fall into place as we construct the correlator  $\left\langle \prod_{i=1}^{N_e} V(z_i, \bar{z}_i) \mathcal{O}_{\text{bg}} \right\rangle$ , where  $\mathcal{O}_{\text{bg}}$  is a suitably chosen background charge and

$$V(z, \bar{z}) = e^{i\sqrt{p+q}\varphi_1(z, \bar{z}) + i\sqrt{p}\varphi_2(z, \bar{z})} \quad (4.4)$$

represents an electron. On the torus, the electron operator  $V(z, \bar{z})$  *can not* be split into a holomorphic part  $V(z)$ , and an anti-holomorphic part  $\bar{V}(\bar{z})$ , therefore the correlator of the full vertex operator needs to be computed. The two fields  $\varphi_1$  and  $\varphi_2$  are two decoupled compactified boson fields with radius  $R_1$  and  $R_2$ , respectively. The correlator is computed as a sum over conformal blocks,  $\left\langle \prod_{i=1}^{N_e} V(z_i, \bar{z}_i) \mathcal{O}_{\text{bg}} \right\rangle = N(\tau) \sum_{E_1, E_2} \psi_{E_1, E_2} \bar{\psi}_{\bar{E}_1, \bar{E}_2}$ . The sum over  $E_1$  and  $E_2$  runs over the points  $E_j = \frac{e_j}{R_j} + \frac{m_j R_j}{2}$  and  $\bar{E}_j = \frac{e_j}{R_j} - \frac{m_j R_j}{2}$  and  $e_j, m_j \in \mathbb{Z}$ . The chiral (and anti-chiral) terms in the sum can be written as

$$\psi_{E_1, E_2} = e^{-\frac{1}{2} \frac{q+p}{q} \sum_i \vartheta_i^2} \prod_{i<j} \vartheta_1(z_{ij} | \tau)^{q+p} \vartheta_1(-\bar{z}_{ij} | -\bar{\tau})^p \mathcal{F}_{E_1, E_2}(Z | \tau).$$

where  $z_{ij} = \frac{1}{L_x} (z_i - z_j)$  and  $Z = \frac{1}{L_x} \sum_j z_j$  is the centre of mass variable. The centre of mass function  $\mathcal{F}_{E_1, E_2}$  is given by

$$\mathcal{F}_{E_1, E_2}(Z | \tau) = e^{i\pi[\tau E_1^2 - \bar{\tau} E_2^2]} e^{2\pi i[E_1 \sqrt{(q+p)Z} - E_2 \sqrt{p}Z]}.$$

The QH wave functions are constructed using only the chiral parts  $\psi_{E_1, E_2}$  of the correlator. Therefore, we now seek linear combinations of  $\psi_{E_1, E_2}$  that have good single- and many-body electron properties. The single-body properties sought are formulated in terms of well-defined periodic boundary conditions under  $t_1^{N_s}$  and  $t_2^{N_s}$ . Applying these operators on  $\psi_{E_1, E_2}$  yields

$$t_1^{N_s} \psi_{E_1, E_2} = (-1)^{N_e - 1} e^{2\pi i[E_1 \sqrt{q+p} - E_2 \sqrt{p}]} \psi_{E_1, E_2}$$

and

$$t_2^{N_s} \psi_{E_1, E_2} = (-1)^{N_e - 1} \psi_{E_1 + \sqrt{q+p}, E_2 + \sqrt{p}}.$$

In order to obtain well-defined phases under  $t_1^N$  and  $t_2^N$ , we must choose a linear combination on the form

$$\phi_{\Gamma, t} = \sum_k e^{tk} \psi_{\Gamma+k(\sqrt{q+p}, \sqrt{p})}. \quad (4.5)$$

Here  $\Gamma = (\Gamma_1, \Gamma_2)$  is the offset from the origin, of the space spanned by  $E_1$  and  $E_2$ . Depending on the choice of  $\Gamma$ , the state  $\phi_{\Gamma, t}$  will have different single-body boundary conditions. Specifying  $\Gamma$

also selects the many-body momentum state of  $\phi_{\Gamma,t}$ . In what follows we will investigate the consequence of choosing different  $\Gamma$ . We will find that different choices of  $\Gamma$  only amounts to choosing different boundary conditions, and changing the coordinate system. In order to see this we will make a rather unusual division of the Gaussian factor as  $e^{-\frac{q+2p}{2q} \sum y_j^2} = e^{-\frac{q+2p}{2q} \sum \tilde{y}_j^2} e^{-\pi(q+2p) \frac{L_x}{L_y} Y^2}$ . Here we have rewritten  $y_j = \tilde{y}_j + \frac{Y L_x}{N_e}$  in terms of the centre of mass coordinate  $Y = \Im(Z)$ , and the relative coordinate  $\tilde{y}_j$ . The relative coordinate is of course chosen such that  $\sum_j \tilde{y}_j = 0$ . By performing the sum over  $k$  in (4.5), we construct the full centre of mass function:

$$\begin{aligned} \mathcal{H}_{\Gamma,t} &= e^{-\pi(q+2p) \frac{L_x}{L_y} Y^2} \sum_k e^{ik} \mathcal{F}_{\Gamma+k(\sqrt{q+p}, \sqrt{p})} \\ &= e^{-\pi(q+2p) \frac{L_x}{L_y} Y^2} e^{2\pi i(\Gamma_1 \sqrt{q+p} Z - \Gamma_2 \sqrt{p} \bar{Z})} e^{i\pi(\tau \Gamma_1^2 - \bar{\tau} \Gamma_2^2)} \times \\ &\quad \times \vartheta \left[ \begin{matrix} 0 \\ t \end{matrix} \right] ((q+p) Z - p \bar{Z} + \tau \Gamma_1 \sqrt{q+p} - \bar{\tau} \Gamma_2 \sqrt{p} | \tau(q+p) - \bar{\tau}(q)) \end{aligned}$$

Note that  $\mathcal{H}_{\Gamma,t}$  is the complete centre of mass function. The expression for  $\mathcal{H}_{\Gamma,t}$  looks rather nasty but can be reformulated. First parametrize  $\Gamma$  as  $\Gamma = r\kappa + s\lambda$ , where  $\kappa = (\sqrt{q+p}, \sqrt{p})$ , and  $\lambda = (\sqrt{p}, -\sqrt{q+p})$ , are two orthogonal vectors. Then  $\mathcal{H}_{\Gamma,k}$  simplifies to

$$\begin{aligned} \mathcal{H}_{t,r,s}(Z, \tau) &= e^{-i2\pi r t} e^{2\pi i s q X} e^{-\pi(q+2p) \frac{L_x}{L_y} Y^2} \times \\ &\quad \times \vartheta \left[ \begin{matrix} r \\ t + sq \Re(\tau) \end{matrix} \right] ((q+p) Z - p \bar{Z} | \tau(q+p) - \bar{\tau} p). \end{aligned} \quad (4.6)$$

To reach (4.6), we also rescaled  $s \rightarrow \frac{qs}{2\sqrt{p}\sqrt{p+q}}$ , and redefined

$$\mathcal{H}_{t,r,s} \rightarrow e^{-i\pi s^2 q^2 [\frac{\tau}{p+q} - \frac{\bar{\tau}}{p}]} \mathcal{H}_{t,r,s}.$$

Although it might not be apparent, the parameter  $s$  is related to a change in coordinates, and therefore to a gauge transformation. This can be seen by shifting  $Z \rightarrow Z + is\Im(\tau)$ . Under this change, the  $sq\Re(\tau)$  term is shifted away, yielding

$$\mathcal{H}_{t,r,s}(Z + is\Im(\tau), \tau) = e^{-i\pi s^2 \Re(\tau)p} \mathcal{H}_{t,r+s,0}(Z, \tau). \quad (4.7)$$

This expression demonstrates that  $s$  is related to a change of the origin of the coordinate system, by  $y_j \rightarrow y_j + \frac{sL_y}{N_e}$ .

Equation (4.7) demonstrates that the different choices of  $\Gamma$  are all related. We may therefore choose  $\Gamma$  to our convenience. The simplest choice  $\Gamma = r(\sqrt{q+p}, \sqrt{p})$ , amounts to  $s = 0$  in (4.6). Under the choice  $s = 0$ , the full modified many-body Laughlin wave function is

$$\begin{aligned} \psi_{t,r}^{(q,p)} &= e^{-\frac{1}{2} \frac{q+p}{q} \sum_i y_i^2} \prod_{i < j} \vartheta_1(z_{ij} | \tau)^{q+p} \vartheta_1(-\bar{z}_{ij} | -\bar{\tau})^p \times \\ &\quad \times \vartheta \left[ \begin{matrix} r \\ t \end{matrix} \right] ((q+p) Z - p \bar{Z} | \tau(q+p) - \bar{\tau} p). \end{aligned} \quad (4.8)$$

The boundary conditions under single-particle translations can readily be found to be

$$\begin{aligned} t_1^{N_s} \psi_{t,r} &= (-1)^{N_e-1} e^{2\pi i r q} \psi_{t,r} \\ t_2^{N_s} \psi_{t,r} &= (-1)^{N_e-1} e^{-2\pi i t} \psi_{t,r}. \end{aligned}$$

By fixing  $r$  and  $t$  we can specify the single-particle boundary conditions. We see that there is a  $q$ -fold freedom in choosing the value of  $r$ . This freedom is related to the  $q$  different possible many-body states. Under many-body translations  $T_1 = \prod_j t_{1,j}$  and  $T_2 = \prod_j t_{2,j}$  the state  $\psi_{r,t}$  transforms as

$$\begin{aligned} T_1 \psi_{t,r} &= e^{2\pi i r} \psi_{t,r} \\ T_2 \psi_{t,r} &= e^{-i 2\pi \frac{t}{q}} \psi_{t, r + \frac{1}{q}}. \end{aligned}$$

These two expressions confirm that  $T_2^q \psi_{t,r} = e^{-i 2\pi t} \psi_{t,r}$ , such that a maximal set of mutually commuting many-body operators constitute:  $H$ ,  $T_1$  and  $T_2^q$ . Here  $H$  is the full interacting many-body Hamiltonian.

By arriving at (4.8), we have succeeded in formulating a torus version of (4.2) with well-defined boundary conditions. However, we can not at this time analytically project  $\psi_{t,r}$  to the LLL, as an analogue of the trick  $\bar{z} \rightarrow \partial_z$  lacking, and the  $\vartheta$ -factors make analytical attempts difficult. In Section 4.2 we will numerically evaluate (4.8), but we will first perform a small sanity check.

To check that the LLL component of  $\psi^{(q,p)}$  depends on  $p$ , we analyse the special case of just one particle ( $N_e = 1$ ) and  $\phi_1 = \phi_2 = 0$ . With only a single particle, there is no Jastrow factor and the modified Laughlin wave function is given by

$$\psi_n^{(q,p)}(Z, \tau) = \mathcal{N} e^{-\frac{q+2p}{2\pi q} y^2} \vartheta \left[ \begin{matrix} -\frac{n}{q} \\ 0 \end{matrix} \right] ((q+p)Z - p\bar{Z} | \tau (q+p) - \bar{\tau}p), \quad (4.9)$$

where  $\mathcal{N}$  is a normalization. It is straight forward to show that the proper normalization of  $\psi_n$  is  $\mathcal{N}^2 = L_x \sqrt{\frac{q\pi}{q+2p}}$ . From there, the overlap with the LLL basis states are calculated to be

$$\langle \eta_n | \psi_m \rangle = \delta_{nm} \left( \frac{1 + 2x}{1 + 2x + x^2} \right)^{\frac{1}{4}}, \quad (4.10)$$

where  $x = \frac{p}{q}$ . Equation (4.10) shows that  $\langle \eta_n | \psi_n \rangle = 1$  when  $p = 0$ , and that  $\langle \eta_n | \psi_n \rangle \rightarrow 0$  as  $p \rightarrow \infty$ . We thus conclude that larger deformations of the Laughlin wave function (larger  $p$ ), has smaller weight in the LLL.

## 4.2 Numerical evaluation of $\psi^{(q,p)}$

Remember that just because the wave functions  $\psi_n^{(q,p)}$  are not entirely in the LLL, this does not mean that they are ill-suited trial wave functions. In their original work, Girvin and Jach noted that the Laughlin state  $\psi^{(q,0)}$  could be improved by considering components with  $p \neq 0$ . On the torus, the same thing is observed. We have numerically compared  $\psi^{(q,p)}$  and the ground state for the Coulomb interaction, by projection  $\psi^{(q,p)}$  on the many-body basis states, in the LLL. Doing so we find, as we expect, that  $\psi^{(q,p)}$  is not entirely in the LLL, for  $p \neq 0$ , but that the projected wave functions  $\mathcal{P}_{\text{LLL}} \psi^{(q,p)}$  still has good overlap with the Coulomb ground state.

The projection of  $\psi^{(q,p)}$  on the LLL is performed using Monte Carlo with importance sampling, and the procedure works as follows: Using  $\psi^{(q,p)}$  as the generating function,  $N$  sets of electron coordinates are chosen using the Metropolis-Hastings algorithm[19]. Then,  $\psi^{(q,p)}$  as well as the many-body momentum basis states are evaluated to get  $N$  data points. The overlap with  $\psi^{(q,p)}$ , and each basis state  $\phi_s$  is computed as

$$\langle \psi^{(q,p)} | \phi_s \rangle = \frac{1}{\sqrt{\mu\nu}} \frac{1}{Z_N} \sum_{i=1}^N \frac{\bar{\psi}^{(q,p)}(x_i) \phi_s(x_i)}{p(x_i)},$$

where  $p(x) = |\psi^{(q,p)}(x)|^2$  is the probability distribution. The normalizing terms are given by

$$Z_N = \sum_{i=1}^N \frac{1}{p(x_i)},$$

and  $\mu = \frac{N}{Z_N}$ , as well as

$$\nu = \frac{1}{Z_N} \sum_{i=1}^N \frac{|\phi_s(x_i)|^2}{p(x)}.$$

The overlap between  $\psi^{(q,p)}$ , and the Coulomb ground state  $\psi_{\text{Coulomb}}$ , is then computed as

$$\langle \psi_{\text{Coulomb}} | \psi^{(q,p)} \rangle = \mathcal{N} \sum_s \beta_s \langle \phi_s | \psi^{(q,p)} \rangle,$$

where  $\beta_s = \langle \psi_{\text{Coulomb}} | \phi_s \rangle$  is obtained from exact diagonalization. The normalization  $\mathcal{N}$  is chosen such that  $\mathcal{N}^2 \sum_s |\langle \phi_s | \psi^{(q,p)} \rangle|^2 = 1$ .

It is possible to perform numerical comparisons for only a small number of electrons, since the dimension of the LLL grows exponentially in the number of electrons. For  $N_e = 3$ , electrons the LLL has 10 many particle states and for  $N_e = 4$  electrons, the LLL has 43 states. These Hilbert spaces are still rather small, but the numerical complexity comes about since the overlap  $\langle \psi^{(q,p)} | \phi_s \rangle$  has to be calculated for all the basis states  $\phi_s^*$ . It is the Monte Carlo sampling of all of these states that take the majority of the time. As the number of electrons are increased, the number  $N$  of Monte Carlo coordinates needed, also increase. This also affects the numerical complexity.

For  $N_e = 3$ , taking  $N = 3 \times 10^6$  Monte Carlo points at  $\tau = \iota$ , the  $(q, p) = (3, 2)$  state has the best overlap with exact Coulomb,  $|\langle \psi_{\text{Coulomb}} | \psi^{(3,2)} \rangle|^2 = 0.9999(4 \pm 6)$  as compared to Laughlin, which has  $|\langle \psi_{\text{Coulomb}} | \psi_{\text{Laughlin}} \rangle|^2 = 0.9990(0 \pm 2)$ .

For  $N_e = 4$ , taking  $N = 3 \times 10^7$  Monte Carlo points, the  $(q, p) = (3, 1)$  state matches Coulomb best, with  $|\langle \psi_{\text{Coulomb}} | \psi^{(3,1)} \rangle|^2 = 0.9976(5 \pm 6)$  compared to  $|\langle \psi_{\text{Coulomb}} | \psi_{\text{Laughlin}} \rangle|^2 = 0.9792(8 \pm 3)$  for the Laughlin state.

We see numerically that we can improve on the Laughlin state at  $\nu = \frac{1}{q}$ , by considering  $\psi^{(q,p)}$  with  $p \neq 0$ . This result is in agreement with Girvin and Jach[6] on the plane.

#### 4.2.1 How to Treat the Derivatives in Many-Particle States

As seen in the previous section, we can write trial wave functions for states in the hierarchy using conformal blocks. On the plane and on the sphere, a trial state can be generated for any rational filling fraction. The method of using conformal blocks and primary operators for describing the electrons, usually results in derivatives, that act on the higher level condensates. The simplest example of this is the case of  $\nu = \frac{2}{5}$ , that has the electron operators

$$V_1(w) = e^{\iota\sqrt{3}\phi_1(w)} \quad V_2(z) = \partial_z e^{\iota\frac{2}{\sqrt{3}}\phi_1(z) + \iota\sqrt{\frac{5}{3}}\phi_2(z)}.$$

We will here use different notation for the electrons described by  $V_1$  and  $V_2$ , to emphasise that not all electrons are treated equally. Because of this asymmetry, the full many-body wave function needs to be antisymmetrized at the very end of the calculation. When calculating the trial wave

---

\*In retrospect, a more effective algorithm would have been to compare with the Coulomb energy eigenstates, as their expected overlap with  $\psi^{(q,p)}$  should fall off with energy. No such statement can be made for the momentum basis states.

functions in a planar geometry, the correlator can be factorized such that the derivatives are outside of the correlator. The trial wave functions are then calculated as

$$\psi = \prod_j \partial_{z_j} \left\langle \mathcal{O}_{\text{bg}} \prod_i V_1(w_i) \cdot \prod_j \hat{V}_2(z_j) \right\rangle.$$

Here  $\hat{V}_2(z)$  is the electron operator without a derivative, such that  $V_2(z) = \partial_z \hat{V}_2(z)$ . As always, a background charge is inserted to make the whole correlator charge neutral. On the torus, things are more complicated, as the correlator can not directly be factorized in a holomorphic and an anti-holomorphic component. Also the treatment of the derivatives is somewhat obscure, as these should now be acting within the full correlator. The approach taken here, is to ignore the external derivatives and insert them first at the very end of the calculation. The correlator can now be calculated, and for  $\nu = \frac{2}{5}$  the linear combination of conformal blocks that fulfils the boundary conditions are

$$\begin{aligned} \psi_s^{(\frac{2}{5})}(\{z\}, \{w\}) &= e^{-\frac{1}{2} \sum_j w_j^2} e^{-\frac{1}{2} \sum_j z_j^2} \mathcal{H}_s(Z^{(1)}, Z^{(2)}) \times \\ &\times \prod_{i < j} \vartheta_1\left(\frac{z_i - z_j}{L_x} \middle| \tau\right)^3 \prod_{i < j} \vartheta_1\left(\frac{w_i - w_j}{L_x} \middle| \tau\right)^2 \prod_{i,j} \vartheta_1\left(\frac{w_i - z_j}{L_x} \middle| \tau\right)^2. \end{aligned} \quad (4.11)$$

The centre of mass function  $\mathcal{H}_s(Z^{(1)}, Z^{(2)})$  is in turn calculated as a combination of conformal blocks

$$\mathcal{H}_s(Z^{(1)}, Z^{(2)}) = \sum_{l=1}^3 (-1)^{tl} \mathcal{G}_{2l}^{(1)}(Z^{(1)}, Z^{(2)}) \mathcal{G}_{5l+3s}(Z^{(2)}),$$

where  $\mathcal{G}^{(j)}$  essentially are  $\vartheta$ -functions, while  $Z^{(1)} = 3 \sum_j z_j + 2 \sum_j w_j$  and  $Z^{(2)} = 5 \sum_j w_j$  [12]. In the  $\nu = \frac{2}{5}$  case, as in general for hierarchy states, all electronic coordinates are not equivalent in the construction and a final antisymmetrization of  $\{z\}$  and  $\{w\}$  is needed.

By evaluating (4.11) we might think, that the problem of constructing a torus trial wave function has been solved; Just put back the derivatives and all will be well. Alas, we are not that fortunate. Since  $[\partial_z, t(\tau L_x)] \neq 0$  the derivatives change the boundary conditions of the  $\psi^{(\frac{2}{5})}$  state and therefore can not be used. But why not skip the use of the derivatives altogether? The answer is, that if we skip the derivatives completely, the antisymmetrized wave functions vanish identically. Some analogue of derivatives must exist to prevent the antisymmetrization from killing the trial wave function.

There is *à priori* no method telling us what should replace the derivatives, when on the torus. There are some constraints that limit the possible alternatives; The wave function should, in the planar  $N_s \rightarrow \infty$  limit, reduce to the planar wave functions; The wave function should transform nicely under modular transformations.

An appealing alternative would be to act with the derivatives, and then project to the LLL. Doing this for one particle, we find the projection to be

$$\mathcal{P}_{\text{LLL}} \partial_z \psi(z) = \frac{1}{2t} \sum_{l=1}^{N_s} a_l t_1^l \psi(z), \quad (4.12)$$

if  $\psi(z)$  is a LLL wave function [4]. The coefficients  $a_l$  are given as the discrete Fourier transform of a piecewise Gaussian function  $G_s$ , defined as

$$G_s = y_s - \frac{L_y}{2\sqrt{\pi}} \sum_t \int_{tL_2 - y_s + \delta}^{tL_2 + y_s - \delta} dy e^{-y^2}. \quad (4.13)$$

Here  $\delta$  is a free parameter describing how the torus is parametrized. The fact that  $\delta$  exists in the final result (4.13), shows that something is pathological, as we do not wish that the final result depends on a parametrization. For the moment, setting aside this caveat about the proper choice of  $\delta$ , we at least obtain a method that translates derivatives  $\partial_z$ , to a well defined operator  $\mathcal{D} = \frac{1}{2i} \sum_{l=1}^{N_s} a_l t_1^l$  on the torus. Applying the recipe  $\partial_z \rightarrow \mathcal{D}$  on the conformal block given by (4.11) we get the many-body wave function

$$\begin{aligned} \Psi_s(\{z\}, \{w\}) &= \prod_j \mathcal{D}_{w_j} \psi_s^{(\frac{2}{5})}(\{z\}, \{w\}) \\ &= \prod_j \left( \frac{1}{2i} \sum_{l=1}^{N_s} a_l t_{1,w_j}^l \right) \psi_s^{(\frac{2}{5})}(\{z\}, \{w\}). \end{aligned}$$

Formally we have managed to obtain a LLL wave function, *but*, it is still pathological. The problem is the many-body operator  $D_w = \prod_j \mathcal{D}_{w_j}$  itself. It is straightforward to verify that  $D_w$  does not commute with any power of  $T_2$ . This non-commutativity is really disastrous, since it means that  $D$  changes the quantum numbers of  $\psi_s^{(\frac{2}{5})}$ , and takes us out of the desired five-fold subspace of trial wave functions. Thus, we can *not* use equation (4.12), even if we find a proper choice of  $\delta$ .

It turns out that the only parts of  $D_w$ , that will commute with  $T_2^5$ , are the parts that can be written as  $T_{1,w}^l$ . Let us just take a moment and clarify the notation. The many-body translation operators acting on the  $w$  and  $z$  coordinates are written  $T_{j,w} = \prod_k t_{j,w_k}$  and  $T_{j,z} = \prod_k t_{j,z_k}$ , such that  $T_j = T_{j,w} T_{j,z}$  act on all coordinates.

To summarize, when constructing states that preserves the  $q$ -fold degeneracy, only certain terms of  $D_w$  are allowed to be kept. The maximally allowed sum of terms may be written as

$$\Psi_s = \sum_{l=1}^{N_s} \alpha_l T_{1,w}^l \psi_s(\{z\}, \{w\}), \quad (4.14)$$

where the parameters  $\alpha_l$  are unspecified for the time being. This ansatz is exactly what was used by Hermanns *et.al.* in Ref. [12]. In their work, they found that as  $L_x \rightarrow 0$ , the first term  $\alpha_1$  becomes increasingly dominant when fitted to the exact ground state for the Coulomb potential.

We now have a problem: We find that when  $L_x$  is changed in the opposite direction, such that  $L_y \rightarrow 0$ , we see that *no* combination of  $\alpha_l$  can give good overlap with the Coulomb ground state. We can understand this result physically by considering the torus geometry. When  $L_x \rightarrow 0$ , the operator  $t_{1,w} \approx 1 + \frac{L_x}{N_s} \partial_x$  approximates a derivative well, since the torus is thin in the  $x$  direction. When  $L_y \rightarrow 0$ , such that  $L_x \rightarrow \infty$ , the torus is thin in the opposite direction. Now, the  $t_{1,w}$  operator does not resemble a derivative any more. We can remedy this by generalizing the ansatz (4.14). We simply trade  $T_1$  for  $T_2$ . These two operators do *not* commute, so  $T_2$  will change the momentum sector of the  $\psi_s$  wave function. This is easily accounted for by letting  $\psi_s \rightarrow \psi_{s-k}$ . We thus get an alternative set of wave functions

$$\Phi_s = \sum_{k=1}^{N_s} \beta_k T_{2,w}^k \psi_{s-k}(\{z\}, \{w\}). \quad (4.15)$$

The numerical overlap with this function and the ground state of the Coulomb potential is bad when  $L_x \rightarrow 0$ , and good then  $L_y \rightarrow 0$ . This is the mirrored behaviour from  $\Psi_s$ , as is seen in

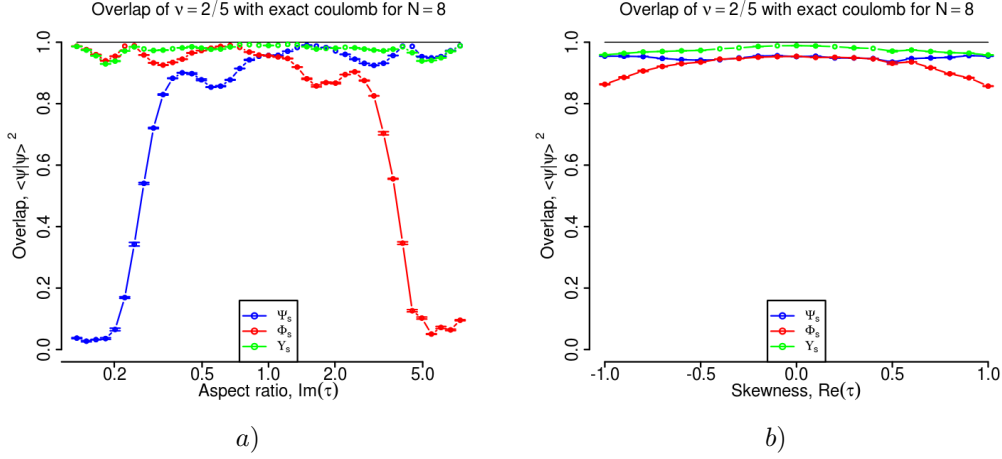


Figure 4.1: Overlap between the exact coulomb ground and  $\Psi_s$  (Blue),  $\Phi_s$  (Green) and  $\Upsilon_s$  (Red), defined in equations (4.14), (4.15) and (4.18).  $\Psi_s$  and  $\Phi_s$  have only  $\alpha_1$  and  $\beta_1$  non-zero. The number of electrons are  $N_e = 8$ . a) Cross section of  $\Re(\tau) = 0$  for  $0.13 < \Im(\tau) < 7.4$ . Notice that the overlap with  $\Psi_s$  drastically vanishes as  $\Im(\tau) \rightarrow 0$ . The mirrored behaviour is seen for  $\Phi_s$  as  $\Im(\tau) \rightarrow \infty$ . The combination  $\Upsilon_s$  is good for all values of  $\Im(\tau)$ . b) Cross section of  $\Im(\tau) = 1$  for  $-1 < \Re(\tau) < 1$ . The combination  $\Upsilon_s$  is still good even though non-trivial phases enter through the coefficients  $\alpha_1$  and  $\beta_1$ .

Figure 4.1a. The general trial wave function ansatz for the  $\nu = \frac{2}{5}$  can thus be extended to

$$\Upsilon_s(\{z\}) = \sum_{l=1}^{N_s} [\alpha_l T_{1,w}^l + \beta_l T_{2,w}^l T_2^{-l}] \psi_s(\{z\}, \{w\}) \quad (4.16)$$

where we write  $\psi_{s-k} = T_2^{-k} \psi_s$ . How can we find some guiding principle that can fix the values of  $\alpha_l$  and  $\beta_l$ ? To find out, we need to study the modular behaviour of the wave function (4.16). In doing so, we will also realize that mixed terms, such as  $T_{1,w}^l T_{2,w}^k$ , will also be needed in the ansatz.

### 4.2.2 The Requirement of Modular Covariance

Modular properties are important since they tell us about how  $\Upsilon_s$  transforms under changes in  $\tau$ . The parameter  $\tau$  encodes information about the geometry of the torus, and thus the space the electrons live on. Since  $\tau$  measures the geometry, or more precisely lets us know which points that are equivalent, there exists transformations of  $\tau$  that should not change the physics. One such transformation is  $\tau \rightarrow \tau + 1$ , also known as a  $\mathcal{T}$ -transformation. Physically this just maps one point of the lattice onto the next point so the geometry of the torus is effectively unchanged, and can be seen in Figure 4.2a.

A second transformation we can perform, is to let  $\tau \rightarrow -\frac{1}{\tau}$ , which is called an  $\mathcal{S}$ -transformation. The  $\mathcal{S}$ -transformation is really a rotation of the torus, by effectively swapping the two axes of the torus, as can be seen in Figure 4.2b. For a rectangular torus it is easily seen since  $\tau = i \frac{L_y}{L_x}$  and  $-\frac{1}{\tau} = i \frac{L_x}{L_y}$  differ by letting  $L_x$  and  $L_y$  trade places. From this simple analysis we can see that when we let  $\tau$  go to  $-\frac{1}{\tau}$  in  $\Upsilon_s$  we will change  $T_1$  into  $T_2$ . That  $\mathcal{S}$  will transform  $T_1$  in  $T_2$  and vice versa is good, since it will constrain the parameters  $\alpha_l$  and  $\beta_l$  in (4.16). We will use



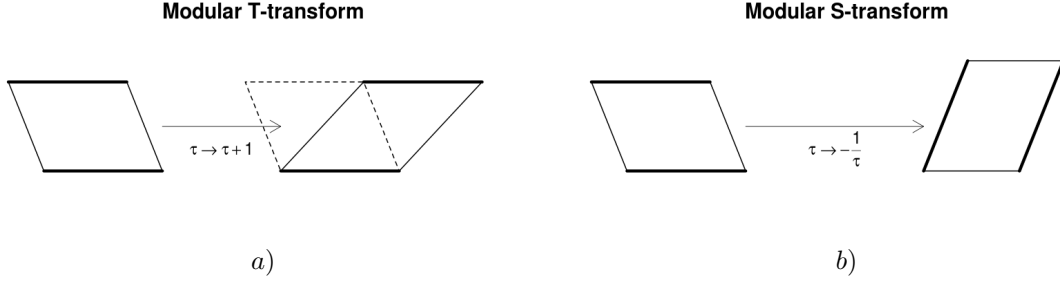


Figure 4.2: a) The geometric interpretation of a  $\mathcal{T}$ -transform,  $\tau \rightarrow \tau + 1$ . Both  $L_x$  and  $L_y$  are unchanged but the torus is tilted such that  $L_\Delta \rightarrow L_\Delta + L_x$ . b) The geometric interpretation of an  $\mathcal{S}$ -transform,  $\tau \rightarrow -\frac{1}{\tau}$ . The torus is effectively rotated such that  $L_x \rightarrow |\tau| L_x$ ,  $L_y \rightarrow \frac{1}{|\tau|} L_y$  and  $L_\Delta \rightarrow -\frac{1}{|\tau|} L_\Delta$ .

that the space of  $\Upsilon_s$  under  $\mathcal{S}$  should transform into itself such that

$$\mathcal{S}\Upsilon_s = \sum_{s'} \lambda_{ss'} \Upsilon_{s'}. \quad (4.17)$$

The complete analysis that fixes the  $\tau$  dependence of  $\alpha$  and  $\beta$  relies on an analysis of the modular transformation properties of the conformal blocks that build  $\Upsilon_s$ . A detailed description of that procedure can be found in Ref. [5], and here we make an heuristic argument of the general behaviour of  $\alpha(\tau)$  and  $\beta(\tau)$ . The numerical results in Figure 4.1 implies that  $\frac{\alpha(\tau)}{\beta(\tau)} \rightarrow 0$  as  $\tau \rightarrow 0$ , and that  $\frac{\alpha(\tau)}{\beta(\tau)} \rightarrow \infty$  as  $\tau \rightarrow \infty$ . The parameters  $\alpha$  and  $\beta$  must thus depend on  $\tau$ , and have certain limiting behaviour. From (4.17) we know that  $\alpha$  and  $\beta$  must transform into each other under  $\mathcal{S}$ , such that  $\Upsilon_s$  has the proper modular behaviour. The last piece of the puzzle comes from a full analysis of how the quasi-particle operators should be regularized in the toroidal geometry. When all of the above factors are taken into account, the coefficients for  $\alpha_1$  and  $\beta_1$  are

$$\alpha_1 = \left( \frac{1}{\vartheta_1\left(\frac{1}{N_s} \middle| \tau\right)} \right)^{\frac{N_e}{2}} \quad \beta_1 = \left( \frac{e^{-i\pi\tau\frac{1}{N_s^2}}}{\vartheta_1\left(\frac{\tau}{N_s} \middle| \tau\right)} \right)^{\frac{N_e}{2}}.$$

The first two terms in  $\Upsilon_s$  are therefore

$$\Upsilon_s = \mathcal{N}(\tau) \left[ \left( \frac{1}{\vartheta_1\left(\frac{1}{N_s} \middle| \tau\right)} \right)^{\frac{N_e}{2}} T_{1,w} \psi_s(w, z) + \left( \frac{e^{-i\pi\tau\frac{1}{N_s^2}}}{\vartheta_1\left(\frac{\tau}{N_s} \middle| \tau\right)} \right)^{\frac{N_e}{2}} T_{2,w} \psi_{s-1}(w, z) \right]. \quad (4.18)$$

In the above equation, the full dependence on  $\tau$  is hidden in the overall normalization  $\mathcal{N}$ .

We can see from Figure 4.1 that the above ansatz gives good overlap with exact Coulomb for all values of  $\tau$ , not only for  $\Re(\tau) = 0$ . This is a non-trivial result since the phases going into  $\alpha_1$  and  $\beta_1$  are strongly fluctuating for a general  $\tau$ . A similar analysis will give us relations between the generic  $\alpha_j$  and  $\beta_j$ . The modular  $\mathcal{S}$  transformation does however not shed any light on the relative size of the different  $\alpha_j$ , so we need another mechanism to fix these. Some numerical work suggest that  $\alpha_j \propto a_j^{\frac{N_e}{2}}$ , where  $a_j$  are the coefficients defined in (4.12), gives an improved

overlap with exact coulomb compared to  $\alpha_j = \delta_{j,1}$ . This is of course a natural guess since the terms in  $\prod_j \mathcal{D}_{w_j}$  that commutes with  $T_2^q$ , have precisely  $\alpha_j \propto a_j^{\frac{N_e}{2}}$  as coefficients.

The  $\mathcal{T}$ -transform introduces further constraints on  $\Upsilon_s$ . Under  $\mathcal{T}$ ,  $\tau \rightarrow \tau + 1$ , the different powers of  $T_1$  and  $T_2$  will transform into each other, such that  $T_2^n \rightarrow T_1^n T_2^n$ . This is easily seen, since what was a translation in the  $\tau$ -direction, will now be a translation in the  $(\tau + 1)$ -direction. That  $T_2$  transforms into  $T_1 T_2$  means that we have to extend the anzats in equation (4.16) to include all combinations of  $T_1$  and  $T_2$ , since they can all be reached by the two modular transformations\*

$$\mathcal{S} : T_1^m T_2^n \propto T_1^n T_2^{-m}$$

and

$$\mathcal{T} : T_1^m T_2^n \propto T_1^{m+n} T_2^n.$$

The extend anzats for  $\Upsilon_s$ , that is covariant under both  $\mathcal{S}$  and  $\mathcal{T}$ , is written as

$$\Upsilon_s = \mathcal{N}(\tau) \sum_{n,m=1}^{N_s} \frac{e^{i\lambda_{n,m}}}{\vartheta \left[ \frac{\frac{n}{N_s} + \frac{1}{2}}{\frac{m}{N_s} + \frac{1}{2}} \right] (0|\tau)^{\frac{N_e}{2}}} T_{1,w}^m T_{2,w}^n \psi_{s-n}(\{w\}, \{z\}), \quad (4.19)$$

where the phase  $\lambda_{n,m}$  is fixed by modular covariance. We do not know, at this time, if (4.19) is the unique solution that respects both  $\mathcal{S}$  and  $\mathcal{T}$  transformations.

As second check that the state (4.19) is properly describing a Quantum Hall fluid, we may calculate the viscosity of that state. In the next Section, this will be done.

---

\* Actually the space of  $T_1^m T_2^n$  terms split into several disjoint but self-similar sets. Two elements  $T_1^m T_2^n$  and  $T_1^{m'} T_2^{n'}$  can only be connected through a combinations of  $\mathcal{S}$  and  $\mathcal{T}$  if their greatest common divisor are the same,  $\gcd(|m|, |n|) = \gcd(|m'|, |n'|)$ .

## Chapter 5

# Viscosity in Fractional Quantum Hall States

As shown before, there are novel difficulties when going to the torus, as compared to the plane. After all, the wave functions are more complicated and there is no clear analogy of what the derivatives are. So why should we bother at all with the torus? We are still interested, because some things are comparatively easy to calculate to the torus, but difficult in other geometries. One such thing is the antisymmetric component of the viscosity tensor. We will soon return to precisely what the antisymmetric viscosity is and how it is calculated.

Our story begins on the sphere. When establishing the filling fraction of a quantum Hall state, the number of fluxes  $N_\Phi$  is compared to the number of electrons  $N_e$ . On the torus,  $N_e$  is proportional to  $N_\Phi$ , such that  $N_e = N_s \nu$ , but this is not true on the sphere. Because of the curved surface, and that the electron has a spin, the electrons will pick up a Berry phase as it moves over the surface of the sphere. This Berry phase will show up as a shift  $\mathcal{S}$ , in the relation between  $N_e$  and  $N_\Phi$ , such that  $N_e = \nu(N_\Phi + \mathcal{S})$ . For the IQHE  $\mathcal{S} = 1$ , but for the FQHE  $\mathcal{S} > 1$ . For the Laughlin state at  $\nu = \frac{1}{3}$ , we have  $\mathcal{S} = 3$  whereas for  $\nu = \frac{2}{5}$ , we have  $\mathcal{S} = 4$ . As such, the shift contains information about the average orbital spin of the electrons  $\bar{s}$ , such that  $\mathcal{S} = 2\bar{s}$ . As different quantum Hall states will have different shifts, it can be used to distinguish these states from each other.

At first glance it looks as if the shift is a purely geometrical effect and has nothing to do with the torus, but this is incorrect. The shift is a topological characteristic of the quantum Hall system, and must thus be observable on all geometries. On the torus, which is a flat surface, the orbital spin does not manifest itself in the filling fraction equation, but rather as a transport coefficient. This particular coefficient is the antisymmetric component  $\eta_A$  of the viscosity tensor. The antisymmetric viscosity is a peculiar thing. Whereas the symmetric viscosity component, the shear viscosity  $\eta_S$ , is related to dissipation, and can be thought of as the *thickness* of a fluid, the antisymmetric component is related to dissipationless response. Simply put, if a system with  $\eta_A \neq 0$  is put under strain, it will start to twist.

The particular type of viscosity we seek to calculate, sometimes called the Hall viscosity, is unique for two-dimensional systems. Avron *et al.* computed the Hall viscosity for filled Landau Levels[2] and found the viscosity to be  $\eta_A = \frac{B}{8\pi}$ . In the case of a partially filled LL, the analysis is more involved, but has been performed by Read & Rezayi for the Laughlin state and the Moore-Read state[22, 23].

Read has demonstrated, that the mean orbital spin is related to the antisymmetric viscosity of the Quantum Hall system[22] as  $\eta_A = \frac{1}{2}\bar{s}\bar{n}\hbar$ . In this simple formula  $\bar{n}$  is the number density

of electrons and  $\bar{s}$  the mean orbital spin of each electron. It is therefore important to calculate the viscosity for the  $\nu = \frac{2}{5}$  trial wave function, to make sure that it is in the right topological phase.

## 5.1 Viscosity in the $\nu = \frac{2}{5}$ State

Considering the  $\nu = \frac{2}{5}$  state, given by (4.19), two things need to be established. First, the overlap with the exact Coulomb ground state has to be high. This will be the first test that the wave function (4.19) is reasonable. As seen in Figure 4.1, depending on whether  $\Im(\tau)$  is small or large, there is either good overlap with  $\Psi_s$  or with  $\Phi_s$  from equations (4.14) and (4.15). Using the combination of both  $\Psi_s$  and  $\Phi_s$ , with the parameters obtained from modular covariance, the combined wave function has good overlap with exact coulomb for all values of  $\tau$ .

We now have two systems for which we may compute the viscosity of the state  $\nu = \frac{2}{5}$ . The exact coulomb ground state, and the Hierarchy state given by (4.19). These systems should both agree with the predicted value of  $\bar{s}$ . We wish to compute the viscosity both for the exact diagonalization and the trial wave functions, because overlap is not the full story.\*

Numerically the viscosity is calculated by evaluating the Berry curvature  $\mathcal{F}$  at a specific  $\tau = \tau_x + \imath\tau$ . We may compute the mean Berry curvature, in a region  $\Omega$  by integrating the Berry connection around a closed loop following the contours of  $\Omega$ . We follow the numerical procedure of Read & Rezayi[23]. The mean Berry curvature  $\bar{\mathcal{F}}$  is obtained from the Berry connection as  $\bar{\mathcal{F}} = \frac{1}{A_\Omega} \oint_{\partial\Omega} A_\mu(\lambda) d\lambda_\mu$ . If the area of  $\Omega$  is small enough,  $\mathcal{F}$  is almost constant, and the path  $\partial\Omega$  may be discretized. As a result  $\bar{\mathcal{F}}$  can be evaluated as

$$e^{\imath A_\Omega \bar{\mathcal{F}}} = e^{\imath \oint A_\mu(\lambda) d\lambda_\mu} \approx \prod_j \langle \varphi_j | \varphi_{j+1} \rangle, \quad (5.1)$$

where  $|\varphi_j\rangle$  is the state at point  $j$ . The area of  $\Omega$  is calculated as

$$A_\Omega = \int_\Omega \frac{d\tau_x d\tau_y}{\tau_y^2} = 2\pi \left[ \frac{\tau_{y,0}}{\sqrt{\tau_{y,0}^2 - \rho_0^2}} - 1 \right], \quad (5.2)$$

where  $\tau_{y,0}$  is the imaginary  $\tau$  coordinate for the centre of  $\Omega$ , and  $\rho_0$  is the radius of  $\Omega$ . The mean orbital spin  $\bar{s}$  can now be calculated as

$$\bar{s} = \frac{1}{2} + 2 \frac{\Re(\bar{\mathcal{F}})}{A_\Omega N_e}. \quad (5.3)$$

The added constant  $\frac{1}{2}$  is the intrinsic spin of the electrons. In general  $\bar{\mathcal{F}}$  has a non-zero imaginary part, if computed through (5.1). That is why explicitly the real part of  $\bar{\mathcal{F}}$  should enter into 5.3.

We calculate the viscosity of the exact coulomb ground state to be  $\bar{s} \approx 2$  for  $\nu = \frac{2}{5}$ , even though the value of  $\bar{s}$  depends on  $\tau$ . This is depicted in Figure 5.1. We believe the  $\tau$ -dependence of  $\bar{s}$  to be a finite-size effect<sup>†</sup>, as it becomes less pronounced for larger values of  $N_e$ .

---

\*There are examples of wave functions, that have very good overlap, they still have very different symmetries. A case in point is the Gaffnian[26], that has good overlap with the exact Coulomb ground state, but also has several pathological properties. One of these properties is the existence of gapless excitations, such that the Gaffnian does not represent a stable gapped topological phase of matter.

<sup>†</sup>It should be noted that for  $\tau \rightarrow \imath 0$  and  $\tau \rightarrow \imath \infty$ , we expect  $\bar{s} \rightarrow \frac{1}{2}$ . In this limit, which is the thin torus limit, all dynamics is frozen out and the problem becomes one dimensional and electrostatic.

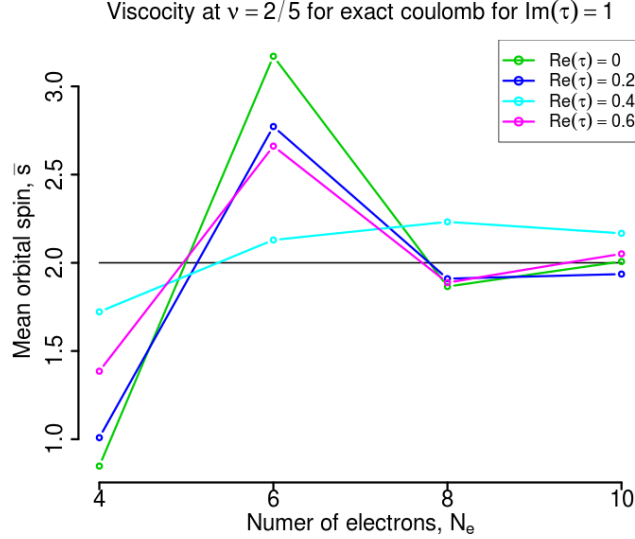


Figure 5.1: Viscosity, in units of the mean orbital spin  $\bar{s}$ , for the exact coulomb ground, with for  $N = 4, 6, 8, 10$  electrons. The torus geometry is  $\Im(\tau) = 0$  and  $\Re(\tau) = 0, 0.2, 0.4, 0.6$ . The different lines correspond to different skewness of the lattice. The value of  $\bar{s}$  depends on  $\tau$ , but it is likely a finite size effect. This is seen since  $\bar{s}$  converge on  $\bar{s} = 2$  as  $N_e$  increases.

We also compute the viscosity for the hierarchical wave function (4.18). There we find that the two components  $\Psi_s$  and  $\Phi_s$  have mutually diverging viscosity in the limit of a thin torus. This is clearly seen in Figure 5.2, where the coefficients entering in (4.18) single out one viscosity value over the other, as expected.

Numerically it is time consuming to evaluate the viscosity. For the exact diagonalization we are as usual limited by the exponential growth of the Hilbert space, meaning that it is not tractable to look at systems larger than  $N_e = 12$ . Also the number of steps that discretize the path  $\Omega$  should be on the order of  $N = 200$  steps, this reduces the largest systems size to  $N_e = 10$ .

For the Hierarchical states there is an added problem. Although we do not need to perform an exact diagonalization, the overlap in (5.1) has to be evaluated using Monte Carlo methods. This introduces statistical noise into the viscosity calculation.

To summarize: The Hierarchy states appear to have the mean orbital spin  $\bar{s} = 2$  expected by studying the shift, although there are still large numerical errors.

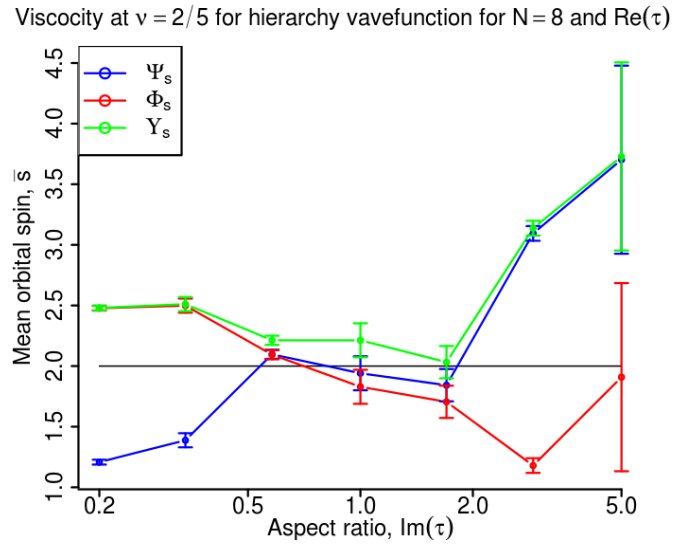


Figure 5.2: Viscosity, in units of the mean orbital spin  $\bar{s}$ , for the Hierarchy wave functions  $\Psi_s$  (Blue),  $\Phi_s$  (Green) and  $Y_s$  (Red) defined in (4.14), (4.15) and (4.18). The torus has the parameters  $\Re(\tau) = 0$  and  $0.2 < \Im(\tau) < 5$ . In the region  $\Im(\tau) \approx 1$  both  $\Psi_s$  and  $\Phi_s$  has viscosity near  $\bar{s} = 2$ . For  $\Im(\tau) \rightarrow 0$  and  $\Im(\tau) \rightarrow \infty$  the value  $\bar{s}$  diverges, both from  $\bar{s} = 2$  and between  $\Psi_s$  and  $\Phi_s$ . It is not clear what is happening in these regimes, but is likely related to the torus becoming thin. It is clear that the different weights in (4.18) are kicking in, as  $Y_s$  follows either  $\Psi_s$  or  $\Phi_s$  depending on  $\tau$ .

## Chapter 6

# Summary and Outlook

In this thesis we have mainly studied the behaviour of coherent states on a torus. Further we have also touched upon the importance of modular invariance when constructing trial wave functions on a torus. We have looked explicitly on two alternative constructions for coherent states. As an application of the coherent states, we have constructed a the torus version of the modified Laughlin  $\nu = \frac{1}{q}$  states, as well as trial states for  $\nu = \frac{2}{5}$ , that is modular invariant. In the case of the  $\nu = \frac{5}{2}$  state, we have calculated the viscosity, and found that it agrees with the predicted value.

The first approach was to project a Dirac  $\delta$ -functions on the LLL. This produced a continuous set of wave functions that by necessity where over-complete. These CCS fulfilled that same kind of resolution of unity and self-reproducing kernel as the coherent states on the plane, and they could be generated in the same way. It is fair so say that the CCS are the torus analogue of the planar coherent states.

The second approach used Haldane and Rezayi's idea to place all zeros at the same point. This generated a family of  $N_s^2$  states where  $N_s$  is the number of fluxes in the system. These LCS wave functions fulfilled relations, similar the resolution of unity and self-reproducing kernel that the CCS possessed. The main difference between the LCS and CCS, except for the number of existing states, turns out to be their localization properties. The CCS approximately minimize the uncertainty relations  $\sigma_x \sigma_y$ , for any value of  $\tau$ , whereas the LCS form two distinct maxima at and around  $\Re(\tau) = \frac{1}{2}$ .

Parts of this thesis deals with using the CCS and/or LCS basis, to project functions that reside in higher Landau levels, down to the lowest one. Interpreting a wave function in a basis of Coherent States, is equivalent to projecting it to the LLL. This is crucial when the trial wave functions contain anti-holomorphic components, such as  $\bar{z}$ . On the plane, these anti-holomorphic coordinates can be interpreted as a holomorphic derivative. On the torus, this interpretation is not possible.

The issue of modular invariance ties in with the problems with derivatives. We have shown that the derivative operator is ill-defined on the torus, and has to be replaced by something else. A naive projection of  $\partial_z$  on the LLL shows that  $\mathcal{P}_{\text{LLL}}\partial_z = \sum_l \alpha_l t_{1,z}^l$ , but since  $\partial_z$  is ill-defined, the coefficients  $\alpha_l$  can not be specified uniquely. We have shown that the many-body states further restrict the values of  $\alpha_l$ , such that only terms of the form  $T_1 = \prod_l t_{1,z_l}$ , will preserve the  $q$ -fold degeneracy of the trial wave functions. Because of modular covariance, we have shown that there must also exist a term with  $T_2 = \prod_l t_{1,z_l}$ . The relative weights of  $T_1$  and  $T_2$  have been calculated from modular covariance.

As a result of the covariance calculation, we have constructed trial wave functions for the

$\nu = \frac{2}{5}$  state. These wave functions have good agreement with the Coulomb ground state, in the entire  $\tau$  plane, already for only one  $T_1$  and one  $T_2$  term. This enabled us to calculate the viscosity of the trial wave function, and find that it coincides well with the values retrieved from exact diagonalization of a Coulomb potential.

Future work will extend the  $T_1$  and  $T_2$  construction to other filling fractions of the hierarchy. Using coherent states we may also construct trial wave functions for filling fractions that can not be reached through only particle condensation.

The antisymmetrization of the  $\nu = \frac{2}{5}$  state poses a numerical problem, as the number of terms that needs to be evaluated grows as  $\binom{2N_e}{N_e} \sim 2^{2N_e}$ . Numerical methods that effectively perform Monte Carlo calculations, using the  $\nu = \frac{2}{5}$  trial wave function, as well as higher hierarchy states, need to be developed.



## Appendix A

# Jacobi Theta Functions and some Relations

All LLL wave functions can be written as a Gaussian part and a holomorphic function. On the torus, which is quasi two-dimensional an natural set of functions to use are the Jacobi  $\vartheta$ -functions. In this appendix we collect the main properties of these functions that will be used throughout the main text. The generalized Jacobi  $\vartheta$ -function is defined as

$$\vartheta \left[ \begin{smallmatrix} a \\ b \end{smallmatrix} \right] (z|\tau) = \sum_{k=-\infty}^{\infty} e^{i\pi\tau(k+a)^2} e^{i2\pi(k+a)(z+b)} \quad (\text{A.1})$$

where  $\Im(\tau) > 0$  for convergence. The zeros of (A.1) are located at

$$z = \frac{1}{2} + m - b + \left( \frac{1}{2} + n - a \right) \tau. \quad (\text{A.2})$$

The  $\vartheta$ -function has two real parameters  $a$  and  $b$  that fulfil

$$\vartheta \left[ \begin{smallmatrix} a+1 \\ b \end{smallmatrix} \right] (z|\tau) = \vartheta \left[ \begin{smallmatrix} a \\ b \end{smallmatrix} \right] (z|\tau) \quad (\text{A.3})$$

and

$$\vartheta \left[ \begin{smallmatrix} a \\ b+c \end{smallmatrix} \right] (z|\tau) = \vartheta \left[ \begin{smallmatrix} a \\ b \end{smallmatrix} \right] (z+c|\tau) \quad (\text{A.4})$$

The two main periodic properties are

$$\vartheta \left[ \begin{smallmatrix} a \\ b \end{smallmatrix} \right] (z+n|\tau) = e^{i2\pi an} \vartheta \left[ \begin{smallmatrix} a \\ b \end{smallmatrix} \right] (z|\tau) \quad (\text{A.5})$$

where  $n \in \mathbb{Z}$  and

$$\vartheta \left[ \begin{smallmatrix} a \\ b \end{smallmatrix} \right] (z+c\tau|\tau) = e^{-i2\pi c(z+b)} e^{-i\pi\tau c^2} \vartheta \left[ \begin{smallmatrix} a+c \\ b \end{smallmatrix} \right] (z|\tau) \quad (\text{A.6})$$

where  $c \in \mathbb{R}$ . Under transformations of the lattice parameter  $\tau$  the relations are

$$\vartheta \left[ \begin{smallmatrix} a \\ b \end{smallmatrix} \right] (z|\tau+n) = e^{-i\pi a(1+a)n} \vartheta \left[ \begin{smallmatrix} a \\ an + \frac{n}{2} + b \end{smallmatrix} \right] (z|\tau) \quad (\text{A.7})$$

where  $n \in \mathbb{Z}$ . Using the Poisson summation formula

$$\sum_{n \in \mathbb{Z}} e^{-\pi a n^2 + b n} = \frac{1}{\sqrt{a}} \sum_{k \in \mathbb{Z}} e^{\frac{(b + 2\pi i k)^2}{4\pi a}}$$

we find that under inversion of the lattice parameter  $\tau \rightarrow -\frac{1}{\tau}$ , the transformation is

$$\vartheta \left[ \begin{matrix} a \\ b \end{matrix} \right] \left( z \middle| -\frac{1}{\tau} \right) = \sqrt{-i\tau} e^{i\tau\pi z^2} e^{i2\pi b a} \vartheta \left[ \begin{matrix} b \\ -a \end{matrix} \right] (\tau z | \tau) \quad (\text{A.8})$$

There is a simple summation rule under Fourier sums

$$\sum_{r=1}^N e^{i\frac{2\pi}{N}rs} \vartheta \left[ \begin{matrix} a + \frac{r}{N} \\ b \end{matrix} \right] (z | \tau) = e^{-i2\pi a s} \vartheta \left[ \begin{matrix} Na \\ \frac{b+s}{N} \end{matrix} \right] \left( \frac{z}{N} \middle| \frac{\tau}{N^2} \right) \quad (\text{A.9})$$

We can define four special cases of the parameters  $a$  and  $b$  that have symmetry properties under  $z \rightarrow -z$ . These functions are

$$\vartheta_1(z | \tau) = \vartheta \left[ \begin{matrix} \frac{1}{2} \\ \frac{1}{2} \end{matrix} \right] (z | \tau) \quad (\text{A.10})$$

$$\vartheta_2(z | \tau) = \vartheta \left[ \begin{matrix} \frac{1}{2} \\ 0 \end{matrix} \right] (z | \tau) \quad (\text{A.11})$$

$$\vartheta_3(z | \tau) = \vartheta \left[ \begin{matrix} 0 \\ 0 \end{matrix} \right] (z | \tau) \quad (\text{A.12})$$

$$\vartheta_4(z | \tau) = \vartheta \left[ \begin{matrix} 0 \\ \frac{1}{2} \end{matrix} \right] (z | \tau) \quad (\text{A.13})$$

where  $\vartheta_1(z | \tau)$  is odd and  $\vartheta_{2,3,4}(z | \tau)$  are even.

# Bibliography

- [1] D. Arovas, J. R. Schrieffer, and F. Wilczek. Fractional statistics and the quantum hall effect. *Phys. Rev. Lett.*, 53:722, 1984.
- [2] J. E. Avron, R. Seiler, and P. G. Zograf. Viscosity of quantum hall fluids. *Phys. Rev. Lett.*, 75:697–700, 1995.
- [3] E. J. Bergholtz and A. Karlhede. Quantum hall system in tao-thouless limit. *Phys. Rev. B*, 77:155308, 2008.
- [4] M. Fremling. Coherent state wave functions on a torus with a constant magnetic field. *ArXiv e-prints:1302.6471*, 2013.
- [5] M. Fremling, T. H. Hansson, and J. Suorsa. Hall viscosity of hierarchical quantum hall states. *In Preparation*, 2013.
- [6] S. M. Girvin and T. Jach. Formalism for the quantum hall effect: Hilbert space of analytic functions. *Phys. Rev. B*, 29:5617, 1984.
- [7] F. D. M. Haldane. Fractional quantization of the hall effect: A hierarchy of incompressible quantum fluid states. *Phys. Rev. Lett.*, 51:605, 1983.
- [8] F. D. M. Haldane. Many-particle translational symmetries of two-dimensional electrons at rational landau-level filling. *Phys. Rev. Lett.*, 55:2095, 1985.
- [9] F. D. M. Haldane and E. H. Rezayi. Periodic laughlin-jastrow wave functions for the fractional quantized hall effect. *Phys. Rev. B*, 31(4):2529, 1985.
- [10] E. H. Hall. On a new action of the magnet on electric currents. *Am. J. Math.*, 2:287, 1879.
- [11] B. I. Halperin. Theory of the quantized hall conductance. *Helv. Phys. Acta*, 56:75, 1983.
- [12] M. Hermanns, J. Suorsa, E. J. Bergholtz, T. H. Hansson, and A. Karlhede. Quantum hall wave functions on the torus. *Phys. Rev. B*, 77(12):125321, 2008.
- [13] J. K. Jain. *Composite Fermions*. Cambridge University Press, 2007.
- [14] C. L. Kane and E. J. Mele. Quantum spin hall effect in graphene. *Phys. Rev. Lett.*, 95:226801, 2005.
- [15] K. v. Klitzing, G. Dorda, and M. Pepper. New method for high-accuracy determination of the fine-structure constant based on quantized hall resistance. *Phys. Rev. Lett.*, 45:494, 1980.
- [16] L. Landau. Diamagnetismus der metalle. *Z. Phys.*, 64:629, 1930.

- [17] R. B. Laughlin. Quantized hall conductivity in two dimensions. *Phys. Rev. B*, 23:5632, 1981.
- [18] R. B. Laughlin. Anomalous quantum hall effect: An incompressible quantum fluid with fractionally charged excitations. *Phys. Rev. Lett.*, 50:1395, 1983.
- [19] M. Metropolis, A. W. Rosenbluth, M. N. Rosenbluth, A. H. Teller, and E. Teller. Equation of state calculations by fast computing machines. *J. Chem. Phys.*, 21:1081, 1953.
- [20] G. Moore and N. Read. Nonabelions in the fractional quantum hall effect. *Nucl. Phys. B*, 360(2-3):362, 1991.
- [21] K. S. Novoselov, A. K. Geim, S. V. Morozov, D. Jiang, M. I. Katsnelson, I. V. Grigorieva, S. V. Dubonos, and A. A. Firsov. Two-dimensional gas of massless dirac fermions in graphene. *Nature*, 438(7065):197, 2005.
- [22] N. Read. Non-abelian adiabatic statistics and hall viscosity in quantum hall states and  $p_x + ip_y$  paired superfluids. *Phys. Rev. B*, 79:045308, 2009.
- [23] N. Read and E. H. Rezayi. Hall viscosity, orbital spin, and geometry: Paired superfluids and quantum hall systems. *Phys. Rev. B*, 84:085316, 2011.
- [24] N. Regnault and B. A. Bernevig. Fractional chern insulator. *Phys. Rev. X*, 1:021014, 2011.
- [25] Wolfgang P. Schleich. *Quantum Optics in Phase Space*. Wiley-VCH, 1 edition, February 2001.
- [26] S. H. Simon, E. H. Rezayi, N. R. Cooper, and I. Berdnikov. Construction of a paired wave function for spinless electrons at filling fraction  $\nu = 2/5$ . *Phys. Rev. B*, 75:075317, 2007.
- [27] H.L. Stormer. Two-dimensional electron correlation in high magnetic fields. *Physica B*, 177(1-4):401 – 408, 1992.
- [28] J. Suorsa, S. Viefers, and T. H. Hansson. A general approach to quantum hall hierarchies. *New J. Phys.*, 13(7):075006, 2011.
- [29] J. Suorsa, S. Viefers, and T. H. Hansson. Quasihole condensates in quantum hall liquids. *Phys. Rev. B*, 83:235130, 2011.
- [30] A. Tzalenchuk, S. Lara-Avila, A. Kalaboukhov, S. Paolillo, M. Syväjärvi, R. Yakimova, O. Kazakova, T. J. B. M. Janssen, V. Fal’Ko, and S. Kubatkin. Towards a quantum resistance standard based on epitaxial graphene. *Nat. Nanotechnol.*, 5:186–189, 2010.
- [31] X.-G. Wen. Theory of the edge states in fractional quantum hall effects. *Int. J. Mod. Phys. B*, 06(10):1711, 1992.